ANL-6717

Argonne National Laboratory

REACTOR DEVELOPMENT PROGRAM

PROGRESS REPORT

April 1963

Price $2.00 . *Available from the Office of Technical Services, Department of Commerce, Washington 25, D.C.*

ANL-6717
Reactor Technology
(TID-4500, 19th Ed.)
AEC Research and
Development Report

ARGONNE NATIONAL LABORATORY
9700 South Cass Avenue
Argonne, Illinois

REACTOR DEVELOPMENT PROGRAM PROGRESS REPORT

April 1963

Albert V. Crewe, Laboratory Director

Division	Director
Chemical Engineering	S. Lawroski
Idaho	M. Novick
Metallurgy	F. G. Foote
Reactor Engineering	B. I. Spinrad
Remote Control	R. C. Goertz

Report coordinated by
R. M. Adams and A. Glassner

Issued May 15, 1963

Operated by The University of Chicago
under
Contract W-31-109-eng-38
with the
U. S. Atomic Energy Commission

FOREWORD

The Reactor Development Program Progress Report, issued monthly, is intended to be a means of reporting those items of significant technical progress which have occurred in both the specific reactor projects and the general engineering research and development programs. The report is organized in a way which, it is hoped, gives the clearest, most logical over-all view of progress. The budget classification is followed only in broad outline, and no attempt is made to report separately on each sub-activity number. Further, since the intent is to report only items of significant progress, not all activities are reported each month. In order to issue this report as soon as possible after the end of the month editorial work must necessarily be limited. Also, since this is an informal progress report, the results and data presented should be understood to be preliminary and subject to change unless otherwise stated.

The issuance of these reports is not intended to constitute publication in any sense of the word. Final results either will be submitted for publication in regular professional journals or will be published in the form of ANL topical reports.

The last six reports issued in this series are:

October 1962	ANL-6635
November 1962	ANL-6658
December 1962	ANL-6672
January 1963	ANL-6683
February 1963	ANL-6698
March 1963	ANL-6705

TABLE OF CONTENTS

TABLE OF CONTENTS

TABLE OF CONTENTS

I. BOILING WATER REACTORS

A. BORAX-V

1. Operations and Experiments

a. Reactor Operations. The core with a central superheater was loaded this month. Sixty boiling fuel assemblies were reloaded into the reactor in reverse order to their last unloading. The critical positions of the reactor controls were determined at intervals of 20, 35, and 60 boiling assemblies containing 40 boron-stainless steel poison rods to confirm that there were no appreciable changes in the core due to the change in core structure and to the removal and reinstallation of control rods and fuel.

Superheater fuel assemblies were then substituted for boiling assemblies. Critical experiments were performed after the substitution of 1, 4, 8, and 12 superheater assemblies. The reactivity effect was negative with the boiler containing 24 poison rods. Figure 1 shows a top view of the core with central superheater fuel installed.

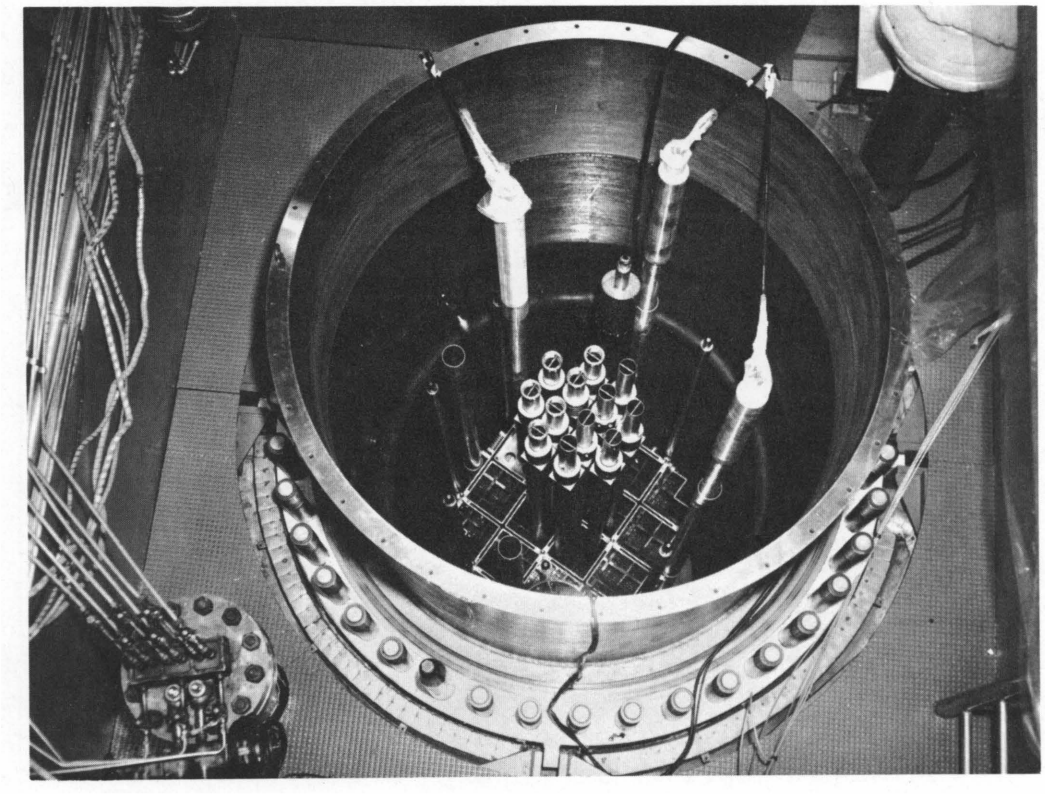

Figure 1. Initial Loading. Central Superheater Core. BORAX-V.

The rod composition of the boiling fuel assemblies was then changed to obtain the maximum allowable excess reactivity for producing power. All of the poison rods were replaced with 4.95 w/o-enriched fuel rods. Water-filled aluminum flow rods were substituted for fuel rods in steps to assure that the reactor did not reach a loading which would be critical on the withdrawal of any single control rod. In the final configuration, each boiling fuel assembly contained 41 fuel rods and 8 flow rods. An accurate determination of the actual value of the available excess reactivity cannot be made until after control rod calibration at operating temperature.

b. Modification and Maintenance. Shims were installed on the structure struts in the central superheater core to produce the desired hold-down force. The 0.039-in.-thick shims will produce an average deflection of the large Belleville spring of 0.090 in. at room temperature and of 0.190 in. at operating temperature (489°F). The resulting forces will be 9000 lb at room temperature and 16,000 lb at operating temperature.

An air motor-driven pump was installed for hydrostatic testing of the reactor vessel and piping systems.

The counting equipment used for gamma scanning of irradiated fuel rods has been modified and checked out.

c. Water Chemistry. Two analytical methods for trace quantities of boric acid were tested. One, the barium chloranilate method, was not satisfactory; the other, using Curcumin, proved to be sensitive to 0.02 ppm and gave acceptable reproducibility with no serious interferences.

Determinations made with water samples from the reactor revealed a concentration of 9 ppm H_3BO_3. Of this, about 5-6 ppm were leaking through the partly exhausted resin bed in the reactor-water demineralizer. The makeup water was found to have a zero concentration of H_3BO_3.

2. Design, Fabrication, and Procurement

a. Experimental Equipment. The detailed design for the acoustic reactor-water-level-probe drive has been completed, and all parts have been ordered. The drive consists of a $\frac{1}{3}$-hp gear motor, driving a position-indicating potentiometer, and a brass nut which drives the threaded probe up and down through a seal on a 6-in. nozzle in the reactor vessel head. Preliminary design of a packing gland-type seal for the level probe is complete.

Detailed design of the fueled oscillator rod is almost complete. This design is similar to the present oscillator except for the fueled rotor, which consists of a 180° arc of uranium-zirconium fuel containing

~100 g U^{235} and a 180° arc of hafnium. The existing oscillator drive will be used with the fueled oscillator. Material for the fueled rotor has been ordered, and the Zircaloy-2 for the housing and rotor end fittings is on hand.

b. In-vessel Instrumentation. A purchase request has been placed with a new vendor for replacement detector coils for the turbine-type flowmeters in the instrumented boiling fuel assemblies. Fabrication of the coils will include machine-welded joints throughout for best reliability.

Additional thermocouples have been ordered for installation in the core entrance and exit regions as detectors for subcooling measurements.

Two sample pieces of W/W-26% Re-sheathed thermocouples were received from the vendor. These pieces utilize ThO_2 insulation in a hard-packed, swaged type of construction. Microscopic inspection of the sheaths indicates a great number of circumferential surface imperfections that average approximately 1 mil by 5 mils along the sheath axis and circumference, respectively. Depth of the flaws appears to be less than 0.5 mil. Longitudinal drawing marks appear on both samples, but the arrangement of flaws is different on the two pieces, which were fabricated at different times. These two samples represent the outcome of an original order placed in May of 1962 for six pieces of material. These two pieces of material are now ready for testing at temperatures up to 5000°F. The remainder of the order has been cancelled, since the vendor's repeated attempts to fabricate the material have been largely unsuccessful.

c. Stainless Steel-clad Superheat Fuel. Atomics International is now fabricating the Type 406 stainless steel-clad enriched fuel plates to be used in two instrumented superheat fuel elements.

Assembly of the plates will be performed at ANL, and assembly parameters are now under investigation. Dummy fuel plates are being nickel plated for use in subassembly brazing development. (The necessity for plating was outlined in the Progress Report for January 1963, ANL-6683, p. 6.)

d. Superheater-water-level-measuring Instrument. A hot-wire, continuous, water-level-measuring system to be used for cold superheater-flooding-time measurements on the superheater has been constructed and tested out-of-pile. The system, based on the use of a 0.0013-in.-diameter wire in the 0.060-in. superheater coolant channel, failed to operate consistently. Testing indicated an apparent tendency for water droplets to cause large errors in the indicated level. It is also believed that surface tension leads to errors because of intermittent support of a column of water in the channel around the wire.

Another design based on an electrical probe to measure change in water resistivity was tried. This system was successful and will be used to give an indication of the empty and full points.

e. Advanced Superheater Fuel Elements. Some fabrication development work on superheater fuel elements made of spherical pellets (see Progress Report for February 1963, ANL-6698, p. 10) is proceeding. Test spheres of UO_2 have been pressed in diameters of 0.355 in. and 0.321 in. A number of these spheres were clad by vacuum-brazing two 0.005-in.-thick hemispherical layers of Type 304 stainless steel with Coast Metals-60 brazing alloy. The equatorial interface of the outer layer is turned 90° from the inner layer. The resulting 0.010-in.-thick cladding is completely coated with the Coast Metals-60 alloy. Eight of these pellets were autoclaved for 2 days at 2700 psi and 680°F with no leaks indicated. Four of the autoclaved pellets and one fresh pellet were corrosion-tested for 2.8 days in deoxygenated steam at 600 psig and 1200°F. One of the previously autoclaved pellets appeared to have a leak; the remaining four pellets exhibited weight gains of from 0.20 to 0.34 mg/cm^2. Only a temper-film type of discoloration was noted.

Cladding hemispheres made of Type 406 stainless steel have been successfully formed by a two-stage draw operation with a pre-and intermediate anneal at 1550°F. Successful welds have been made on hemispheres of 0.010-in.-thick Type 304 stainless steel by both the electron-beam and tungsten-inert-gas processes. However, these two welding methods do not appear amenable to mass production. Resistance welding of 0.010-in. hemispheres of Type 304 stainless steel in a vacuum gave a good bond at the interface, but resulted in holes through the cladding adjacent to the weld zone.

A Plexiglas flow test mockup of two advanced superheater fuel assembly configurations, the "pea-in-a-pod" and the spherical pellet, is being designed. Plastic balls, 0.312 in. and 0.375 in. in diameter for each respective design have been procured. Pressure-drop tests will use the air system of the existing air-water loop.

3. Operator Training

The BORAX-V Systems Training Course for six recently hired technicians has been completed. Fifteen classroom hours were spent in training this month.

B. Metallographic Examination of Fuel-plate Samples from SL-1

A number of samples from several fuel plates from the SL-1 reactor were obtained to study the degree of damage which occurred in the fuel as a result of the excursion which resulted in destruction of the reactor. The items of particular interest were the performance of the X8001 aluminum alloy cladding with respect to corrosion and to the silicon-bond at the core interface, and the metallographic appearance of the fuel in both damaged and undamaged areas.

Since the samples as received were not identified according to their position within their respective specimen groups, several samples from each group were examined and the results considered as representative of the area involved. In addition, since no dimensions were available as to the position of each group of samples relative to the respective plate, it was possible only to generalize as to the lowest point at which melting occurred.

It was found that the structure of the fuel alloy (Al-17.5 w/o U -2.0 w/o Ni-0.5 w/o Fe) did not change in appearance near the bottom end closure of any of the plates, but did experience various degrees of change as a result of melting in the upper heat-affected zones. The appearance of the core in these areas was characterized by a central melted fuel area of varying thickness surrounded on either side by unaffected core alloy. Cracks extended from the center region to the core-clad interface, being filled in most cases with recrystallized fuel. These cracks apparently resulted from the high internal stresses developed in the fuel during the transient. Reaction between the fuel particles and the matrix also occurred in these areas, although none occurred between the fuel and the matrix at the bottom end closure. The rather sharp demarcation between the center area and the surrounding unaffected core alloy affirmed that the melting was of an instantaneous nature rather than a prolonged occurrence. Although, as mentioned previously, it was not possible to pinpoint the beginning and ending of melting within each fuel plate due to lack of information on sample location, it could be determined by consideration of sample size and relative position within the plate that melting began at 3 to 5 in. from the lower end of the plate.

The silicon-bonded interface between the aluminum-uranium core and the X8001 aluminum alloy cladding did not show any signs of deterioration. Measurement of the core and cladding thicknesses revealed that the cladding did not experience any significant degree of corrosion. The core thickness remained within close limits near the lower end closure, but varied between wide limits in areas where fuel melting had occurred. This variation in thickness is apparently due in part to the extrusion of molten core through openings in the plate with subsequent collapsing of the cladding.

II. LIQUID-METAL-COOLED REACTORS

A. General Research and Development

1. ZPR-III

Assembly 43, the second two-zone reactor constructed in ZPR-III, consists of a dilute central core representing a 4,000-liter, sodium-cooled power reactor, a radial buffer region, and an annular driver. A cross section of the core is shown in Figure 2.

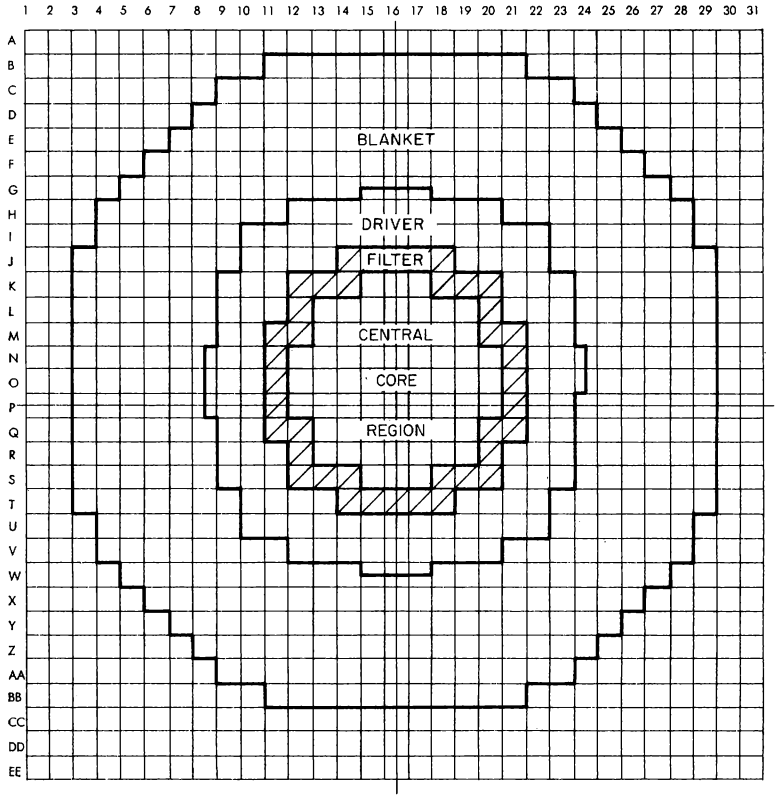

Figure 2. Outline of Core, Assembly 43

This assembly is of particular importance because no present critical facility is capable of mocking up a 4,000-liter power reactor core. The driver-filter concept reduces the mockup to a manageable size while maintaining the highly degraded spectrum in the center of the core region. This allows the measurement of spectral indices and reactivity effects due to material replacements. Also, since the spectrum in the central region is the most highly degraded of any assembly so far built in the ZPR-III, the possibility of performing a meaningful Doppler experiment is enhanced.

a. Physical Description. The central core region is 34.06 in. long and roughly circular in cross section. The drawer loading consists of five

$\frac{1}{4}$ in. sodium cans, three $\frac{1}{8}$ -in. columns of depleted uranium, two $\frac{1}{8}$ -in. columns of graphite, one $\frac{1}{16}$ -in. column of stainless steel, and one $\frac{1}{16}$ -in. column of 93% enriched uranium. The low-density axial blanket behind the central region is identical to the core except that the enriched uranium is replaced with stainless steel. However, the sodium inventory was insufficient, and 45%-density aluminum was used to simulate sodium in the last three inches of the axial blanket in Half No. 1. This is illustrated in Figure 3, a vertical section along the cylindrical axis of the assembly.

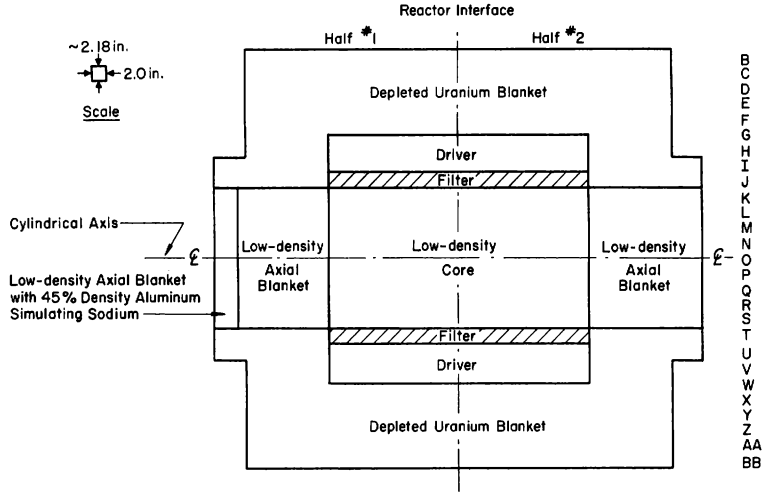

Figure 3. Vertical Section of Assembly 43 through Column 16 of the ZPR-III Matrix

The filter has the same length as the central region and is at least one drawer thick throughout. The loading consists of nine columns of depleted uranium and seven columns of graphite loaded alternately to form a nearly homogeneous mixture in each drawer. The driver is loaded to the same length as the core and filter regions with eight columns of graphite, six columns of stainless steel, and two columns of 93% enriched uranium.

The filter and driver are completely blanketed with depleted uranium. However, since the low-density axial blanket is fairly transparent to neutrons, it was loaded to the end of the blanket drawers; and an additional annular region of depleted uranium was extended to maintain continuity in the radial direction. This is also illustrated in Figure 3. The composition and physical properties of the assembly are listed in Table I.

b. Experimental Results

(i) Critical Mass. Assembly 43 went critical with 72.062 kg U^{235} in the central region, 1.879 kg in the filter, and 515.062 kg in the driver, with the control rod withdrawn 3.092 in. The rod was calibrated (total worth about 86 Ih), and the worth of edge driver material was measured as 29.2 Ih/kg U^{235}. With this measurement, the just-critical mass, including the U^{235} in the filter region, is 588.1 kg U^{235}.

Table I. Composition and Physical Properties of Assembly 43

	Core	Low-density Axial Blanket	Filter	Driver	High-density Blanket
Outer radius (cm)	24.40	24.40	31.39	45.26	~75.
Length (cm)	86.51	38.1 each end	86.51	86.51	38. [a], 27.9[b]
Volume (l)	161.72	71.35	106.05	288.98	-
Volume Fractions					
U^{235}	0.02376	0.000637	0.000945	0.09506	0 0019
U^{238}	0.1523	0.1523	0.4518	0.006775	0 8330
C	0.09936	0.09936	0.3478	0.3935	-
Na	0.4820	0.4820[c]	-	-	-
SS	0.1940	0.4346	0.09092	0.400	0 0731
Atomic Density (atoms/cm^3) x 10^{24}					
U^{235}	0.001141	30.59×10^{-6}	0.000045	0.004563	0.0)00912
U^{238}	0.007309	0.007309	0.02169	0.000325	0.03998
C	0.008326	0.008326	0.02914	0.03297	-
Na	0.01060	0.01060[c]	-	-	-
SS	0.01643	0.02086	0.00770	0.03388	0.0)619

[a] Length of the extended high-density axial blanket.

[b] Normal length of high-density axial blanket.

[c] The quoted values are for that part of the axial blanket which does not contain aluminum.

(ii) Traverses. Both axial and radial traverses for reaction rate were performed with U^{234}, U^{235}, U^{238}, Pu^{239}, and BF_3 counters. The axial traverses were performed in locations 1-0-16 and 2-0-16, starting in Half No. 2 and extending part way into Half No. 1. The radial traverses were performed through column 16, $\frac{1}{2}$ in. back from the interface in Half No. 2. The resulting data are being processed.

(iii) Spectral Measurements. Central fission ratios were measured for U^{233}/U^{235}, U^{236}/U^{235}, and U^{238}/U^{235}. Additional measurements will be completed later. Spectral measurements were also made with a Li^6 solid-state detector. Measurements were made at the core center, in the axial blanket, and in the driver region. These data are also being analyzed.

(iv) Doppler Measurements. Presently, experimental Doppler-measuring equipment is being assembled and fitted into the ZPR-III facility. This will be used for a preliminary experiment to determine if the experimental equipment and technique will, in fact, lead to a result which can be attributed to the Doppler effect.

2. Preparations for ZPR-VI and ZPR-IX Operations

a. ZPR-VI. The ZPR-VI facility is still being held in standby condition ready to operate as soon as approval of the Reactor Safety Analysis Report (submitted to the AEC in August, 1962) is received.

b. ZPR-IX. The aluminum matrix tubes have been redrawn and are ready for bundling into five-by-five arrays. Nine bundles were assembled and stacked on the ZPR-IX bed to form a matrix of full height and one bundle wide. The bundles were loaded with uranium-filled drawers having an average density corresponding to one-fourth of a full loading. The inside heights of a number of empty tubes located at various elevations in the matrix were measured before and after loading. In no case did any tube deflect to an inside height less than the nominal inside dimension of the tubes. This indicates that any observed deflections merely represented the takeup of initial curvature and there would be no binding of control rods under normal load.

During these tests it was noticed that the drawers sliding within the tubes were scored and abraded. This scoring was caused by rough spots in the weld areas. The rough areas will be eliminated. The application of a hard anodizing film on the sides of the drawer is being considered as a possible means of decreasing friction.

Initial tests performed with constrained sections of aluminum matrix tubes loaded by pressure from a hydraulic press (see Progress Report for March 1963, ANL-6705, p. 15) indicated a decrease in the inside height of the tubes of about 0.5 mm, and about twice this for unconstrained tubes, for a loading corresponding to the full height of a matrix loaded with uranium. Much of this deflection occurs with the first few kilograms of load and represents the takeup of the initial outward curvature of the tube walls. Ultimate failure of the samples occurred at loads equal to about $3\frac{1}{2}$ times the above-mentioned full load for the unconstrained samples and at about 10 times for the constrained samples. The tubes are normally used in the constrained position between massive side supports on the table.

Inspection of the aluminum drawers received from the vendor indicated that they did not meet dimensional specifications, and the drawers have been returned for corrective rework.

Individual testing of the safety rods and the dual-purpose rod drives has begun.

c. Experimental Preparation. Specifications are being prepared for the fabrication of beryllium oxide, uranium oxide, vanadium, niobium, and additional enriched uranium plates for use on the ZPR-VI and ZPR-IX facilities.

A mechanical oscillator for use in Doppler effect measurements has been fabricated and checked out on the facility. The electronic timing circuits for the oscillator are being designed.

An electronic reactor period simulator is being designed for checking the response of period-measuring instrumentation. The device will provide simulated ionization chamber currents with periods from less than one to about 5000 sec with an accuracy of 0.5% or better.

B. EBR-I Mark IV

Foil irradiations for the determination of the production of Pu^{239} from U^{238} and for the destruction of U^{235}, U^{238}, and Pu^{239} by fission in Mark IV were completed in March.

To interpret the relative measurements on an absolute basis, and hence to establish a value for the breeding ratio, it was necessary to irradiate simultaneously Pu^{239}-, U^{235}-, and U^{238}-calibrating foils at specific monitoring locations. Duplicate sets of foils were irradiated for approximately one hour at 10 kw. One set, including aluminum-clad Pu^{239} foils, was sent to the analytical group at the Idaho Chemical Processing Plant for radiochemical analyses. The other set, without Pu^{239} foils, was analyzed by an analytical group at the Laboratory. Both groups carried out radiochemical measurements of the total number of fissions and capture in the U^{238} foils and the total number of fissions in the U^{235} foils. The CPP group also reported the total number of fissions in the Pu^{239} foils. The two sets of independent results, however, failed to agree within an acceptable margin of error. The reasons for the various discrepancies are not known. Both groups are presently reviewing their methods in an effort to establish the source of difficulty. At some appropriate point in the current oscillator studies, a second foil calibration run will be made. Foils irradiated in this run will again be sent to the same groups for analysis. To eliminate the possibility of flux depression and self-protection effects, duplicate sets of foils will not be irradiated. Single foils of enriched and depleted uranium will be irradiated and split into halves, with one half being sent to each group.

Transfer-function measurements at zero power have been completed. As part of a program to compare relative speed, reproducibility, and accuracy, independent measurements were conducted with the conventional null-balance system and the Fourier analyzer (cross-correlation technique). A smooth best-fit curve drawn through the various data points permits the following conclusions: (1) for frequencies greater than 0.04 cps, the agreement between amplitude data is excellent; (2) for frequencies less than 0.04 cps, amplitude measurements with the Fourier analyzer fall consistently below the best-fit curve by approximately 1-2%, while the corresponding

null-balance data points fall consistently above the best-fit curve by about 2%; and (3) both systems lead to phase data which are consistent over the entire frequency range. Since the amplitude discrepancies are not large, particularly in the frequency region of interest, the decision was made to accept the best-fit smooth curve through all data points as the reference zero-power curve.

Following the zero-power calibration runs, a cautious approach to higher levels of power was undertaken. To test for evidence of a prompt, positive power coefficient, component flow-change tests, supplemented with power-coefficient measurements, were undertaken at approximately 300 kw. No evidence of a prompt positive component was noted. This information, coupled with the knowledge that the steady-state power coefficient was strongly negative, permitted an increase in power to 510 kw. Again, flow-change tests were conducted, with the result that no evidence of a prompt positive component was found. Power-coefficient measurements resulted in a value of 0.175 Ih/kw evaluated over the region from 316 to 510 kw. As a basis for comparison, similar measurements conducted with Mark III resulted in a value of 0.145 Ih/kw. Because of the lower value of the effective delayed-neutron fraction, the power coefficient for the Mark IV core represents a lower value of power coefficient.

Using the null-balance technique, amplitude and phase data were obtained over the frequency range from 0.02 to 10.0 cps at full flow, low inlet temperature, and power levels of 510 and 900 kw. The results of these measurements permit the following conclusions: (1) under these conditions, the reactor is extremely stable to small oscillating inputs of reactivity; and (2) the feedback is of a type which, if linear, would indicate stability at designed operating power.

After initial operation of the reactor for approximately 2 hr at 500 kw, at low temperature (50°C) of the coolant at the inlet, and a maximum fuel temperature of 170°C, a loss of 20 Ih reactivity was measured. No further changes in reactivity were noted during operation at 500 kw and low inlet temperature.

After raising the temperature of the coolant at the inlet to 200°C, the central fuel temperature reached 316°C at a reactor power of 500 kw. Following operation at high inlet temperature at this power for 3.5 hr, the reactor was cooled down. An increase of 91 Ih was measured in the cold critical position. After an additional 9 hr of operation at high temperature, the reactor was again cooled down, and the cold reactivity increase was measured to be 5 Ih. This indicates that the reactivity changes due to operation at high inlet temperature and 500 kw have become very small and the reactivity is almost stabilized for these operating conditions.

The reactor power was then increased to 900 kw at low inlet temperature for 4 hr. Upon shutdown, the cold critical position showed a reactivity loss of 51 Ih. After an additional 7 hr of operation at 900 kw and low inlet temperature, an additional loss of 6 Ih was measured. The reactor control positions after reaching 900 kv were consistent with the temperature level of the reactor and indicated no large reactivity change after reaching this power. Operation will be continued to investigate the cause of the changes in reactivity.

C. EBR-II

1. Reactor Plant

Difficulty has been encountered in the operation of the No. 1 primary sodium pump. This is one of two identical units purchased from an outside vendor and tested in a water loop prior to installation in EBR-II. The difficulty arose during initial operation. The procedures for initiating operation of the pumps began on April 15 when the vendor's representative arrived at EBR-II. After correction of certain minor difficulties in the power supplies and control systems, the two units were placed in operation at low speed. Difficulty was encountered with the motor-generator set for Pump No. 1 and operation was suspended. This involved disassembly of the Dynamatic coupling and while this work was in progress, operation of Pump No. 1 was attempted by connecting it to the motor-generator set for Pump No. 2. The pump failed to operate and the cap was removed from the top of the drive motor. Torque of 200 ft/lb was applied manually to the pump shaft but it did not turn. On April 20, the shaft was rotated manually through 360° with about 600 ft/lb torque. Through about 20° of rotation the pump turned freely (approximately 2 ft/lb torque). At all positions of rotation the pump shaft and motor shaft, coupled to form an integral unit, could be moved vertically. The motor was then removed and it was determined that the motor shaft rotated freely and that the difficulty was in the pump shaft. The first tests indicated that the pump shaft was warped or bowed and that it would turn freely only if the upper end were permitted to rotate in an oscillatory motion with a radius slightly in excess of $\frac{1}{16}$ inch. An effort was made to determine if a position could be found at which the upper end of the shaft could be constrained on a fixed center line and yet permit free rotation of the shaft. This was found to be impossible.

Secondly, an effort was made to remove or reduce the amount of bowing in the shaft by peening its uppermost weld preferentially. (Note- this weld is approximately five feet below the upper end of the shaft and the peening operation was performed under extremely restricted conditions.) Initially it appeared that the peening was improving the condition slightly, but it was then found that the shaft nominal center line was changing. It was found that by prying the top of the shaft in any direction it could shift the apparent center line between approximately .050 to .100 inch, depending upon the

direction. In response to our inquiry, the vendor has suggested that they believe the impeller may be loose on the shaft and since the lower bearing is integral with the impeller, this would account for the slight shifting of the shaft center line. It thus appears that two problems may exist:

(1) The shaft is bowed or warped, and

(2) The impeller is loose on the shaft.

Although there is some possibility that the first condition could be accommodated by a special eccentric coupling between pump shaft and motor shaft, there is no solution to the second problem except to remove the pump and correct the condition.

Design and procurement of the special equipment required to effect removal of the pump is proceeding. Removal will be a relatively complex operation because it must be done without violating the inert gas atmosphere above the sodium in the primary tank. It also is necessary to protect the immersed sections of the pump from normal building atmosphere during this operation. The major pieces of equipment involved will include:

(1) A spool piece which will provide an adapter to the pump nozzle in the primary tank and effect the atmosphere seal at that point.

(2) A "silo" which connects to the top of the spool piece and serves as an inert atmosphere caisson into which the pump will be withdrawn.

(3) A tank or envelope into which the pump will be placed for cleaning and/or disassembly operations.

During the removal operation the pump and the primary tank sodium must be blanketed at all times with argon gas. An internal closure in the spool piece must be provided to permit isolating the primary tank after the pump has been withdrawn. A second closure is required to close the bottom of the silo during transport of the pump to the cleaning tank. The sodium in the primary tank will be cooled to approximately 250°F (approximately 40°F above the melting point), prior to pump removal. The pump will be cooled to approximately room temperature inside the silo prior to transport.

In addition to the removal equipment, a temporary shield plug will be required to replace the pump during the period it is out for repair. This unit will be designed to perform two functions: (1) to close the pump nozzle in the primary tank cover with adequate thermal insulation to permit raising the sodium temperature to 700°F; and, (2) to provide a closure to the reactor inlet pipe normally fed by this pump. This closure is necessary to enable sustained operation by Pump No. 2. It should be noted that the two pumps

operate in parallel and that there are no check valves in the system. Pump No. 2 cannot be operated except for short test periods until Pump No. 1 has been removed and the pipe closed off. With the latter conditions about three fourths of full reactor flow can be achieved.

During the time that the removal equipment is being fabricated, the primary tank temperature will be maintained at 650°F and fuel handling operations will be continued, including the check out of special operations. During this period the neutron source will be installed in the reactor which will permit the calibration and checkout of neutron instrumentation. Approximately one week before pump removal is to begin, cooling of the sodium will be initiated to slowly reduce the temperature to approximately 250°F. After the pump has been removed and replaced by the temporary shield plug, the primary sodium will be slowly increased in temperature to 650°F Circulation of sodium will then be resumed with one pump and the schedule of operations which has been interrupted will be resumed. Simultaneously, Pump No. 1 will be disassembled and correction of the problems will be effected after the cause has been definitely ascertained.

In summary, present plans are based on the objective of removing the defective pump as soon as possible and providing a replacement plug which will permit "near normal" operation of the system. It is intended that the system will be adequate to permit all operations to be performed through Wet Critical. The only requirement for pumping during the Wet Critical experimental program is to ascertain if any hydraulic effects can be noted on the reactivity of the system. It is believed that this can be observed adequately with one pump in operation (flow distribution through the reactor is essentially unchanged from two pump operation). The repaired pump can, of course, be reinstalled at an earlier date if this appears advisable.

Work unassociated with the pumps accomplished during the period included the following items.

The permanent sodium purification system was placed into operation with its modified surge tank and is currently undergoing checkout Numerous plugging temperature indications were obtained on both the permanent and the temporary purification systems. These indications agree with the results of several "vacuum distillation" analyses and show the oxide concentration of the primary sodium to be close to 10 ppm.

Initial testing of the fuel unloading machine and its temporary argon cooling system was completed satisfactorily. Also, minor adjustments to fuel handling mechanisms were made to improve their alignment at present (normal operating) temperatures. It was found necessary to add a small extension ring to the lower end of the fuel unloading machine gripper body to aid in the manual operation of transferring a subassembly to the gripper

from the transfer arm without interference occurring. After this, the two "fill-filter" subassemblies (one in the core and the other in the outer blanket) were removed from the primary tank without difficulty and were replaced by a filter subassembly and a regular outer blanket subassembly.

The reactor vessel cover lock mechanism reported earlier to be mechanically bound was repaired and placed back into operation. Special fixtures were fabricated which enabled the mechanism to be partially withdrawn from the primary tank, partially disassembled, reworked, and again lowered into position without reducing tank temperature (650°F) or permitting significant inleakage of oxygen. The trouble was found to stem from a galled upper tie rod shaft bearing. This defective bearing was removed, the shaft surface reconditioned, and a new bearing installed (the bearing material was changed from Stellite to aluminum-bronze). Since reinstallation, the lock has been operating properly.

Work is continuing toward modification of the temperature controllers and air-flow distribution system to achieve desired temperature spread in the liquid metal of the seal troughs of the small and large rotating plugs. Figures 4 and 5 show typical temperature distributions around the circumference of these troughs for the half-molten condition of the Cerrotru alloy (42.0% tin and 58.0% bismuth).

In this condition, maintained during reactor operation, the lower half of the alloy is kept molten to minimize argon leakage, while the upper half is maintained solid to provide maximum containment in the primary system.

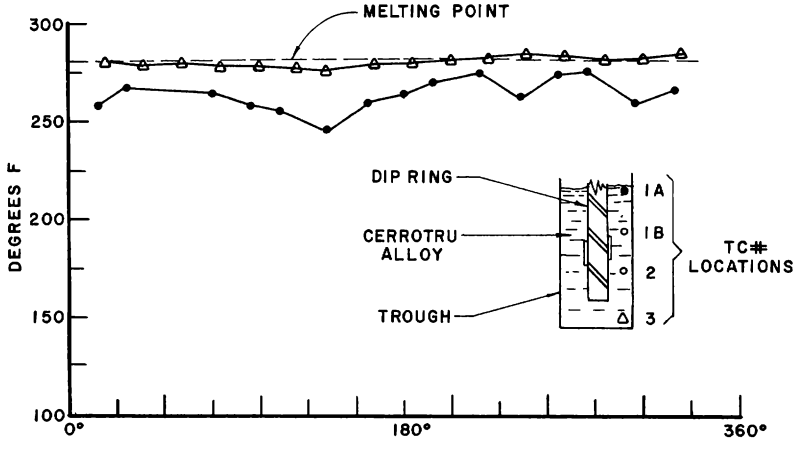

Figure 4. Circumferential Temperature Distribution, Seal Trough, Small Rotating Plug, EBR-II

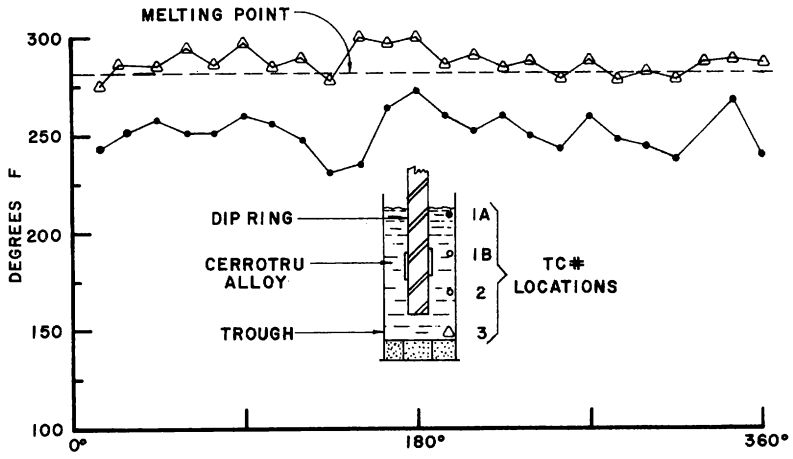

Figure 5. Circumferential Temperature Distribution, Seal Trough, Large Rotating Plug, EBR-II

The desired solidus-liquidus interface is achieved by controlling the operation of several levels of electric heaters installed around the perimeter of the plugs in their respective dip rings (see Progress Report for August 1962, ANL-6610, p. 25). The temperature at different levels is regulated by scanning-type controllers which measure the individual thermocouple outputs sequentially and effect "ON-OFF" power states to regulate the temperature of the seals. The variation in temperature shown on the curves is accounted for by the differences in design of structure adjacent to the trough and by variation in air-cooling flow to the shield-cooling system.

2. Sodium Boiler Plant

Removal from the site of the railroad tank cars used to fill the sodium system was accomplished by the vendor.

Replacement of relays on the Panascan panel to control induction and resistance heaters was completed.

Sampling of argon cover gas from a sodium storage tank and the secondary system piping continued. Initially, the hydrogen content of the sodium piping system exceeded 2000 ppm. On two different occasions, the secondary piping system was purged by pressurizing and bleeding. The hydrogen content of the gas decreased following each of the purges, averaging 1500 ppm after the first and 925 ppm after the second.

Dew-point measurements were taken in the supply main, in the secondary piping system, and in the cover gas over the sodium in the storage tank. These were -95°F, -20°F, and -60°F, respectively. The -20°F dew point indicates about $\frac{1}{2}$ fluid ounce of water in the form of vapor in this system.

A vacuum pump was connected to the storage tank and a vacuum of 18-in. Hg effected on both the tank and the piping. The system was refilled to 3 psig with argon and, after 12 hr, tested for hydrogen. Two samples indicated 173 ppm and 185 ppm hydrogen.

The system will be allowed to remain in its present condition during further testing for possible hydrogen and moisture changes.

3. Power Plant

The major accomplishment on the steam system during the period was the adjustment of piping hangers on the yard blowdown, feedwater, and steam lines to assure proper drainage. This was necessary to prevent the freezing of water in outside piping during periods of shutdown during the winter.

Actual measurements on the system indicated that a total pitch for the 3-in. blowdown line was 4.6 in; for the 6-in. feedwater line, the total pitch was 4.9 in.; for the 10-in. steam line, the total pitch was about 1 in. Due to the relative size of these lines, acceptable draining is now anticipated.

Additional instrumentation was installed, and modifications to the condensate system have been checked and found to be satisfactory.

The steam system is now ready for the forthcoming fill with sodium of the secondary system and the ensuing heatup to 580°F.

4. Fuel Cycle Facility

Modification to the carriages and bridge drive units of the three in-cell cranes has been completed. These units now meet the criteria of interchangeability and remote maintenance. The cranes have been returned to operational status.

The glove boxes for sodium handling have been brought to operational status. The argon-purification system for the glove boxes has been leak-tested and placed in operation. System instrumentation indicates the present argon atmosphere contains 24 ppm water and 4 ppm oxygen. The 24-ppm water content is expected to drop during the next month as complete outgassing of the system proceeds. Basic equipment for the sodium loading of fuel pins and for the carbon-in-sodium analysis work has been installed.

Arrivals of equipment during the month included the two pin-processing machines and spare parts for each operation, the pallet-loading station, the furnace-charge table, the fuel-assembly table, and the Argon Cell periscope.

The pin-processing machine, shown in Figure 6, demolds and shears fuel pins, sorts them by length, weighs them, measures their diameters, and detects flaws in the pins. The components are replaceable, and those performing a given function in one machine are interchangeable with their counterparts in another. Balanced pickup lugs were provided to facilitate the installation of components by manipulators, and lifting tools and porter bars were designed and tested for those components which are replaceable. The assembly of these machines by remote operation has been demonstrated.

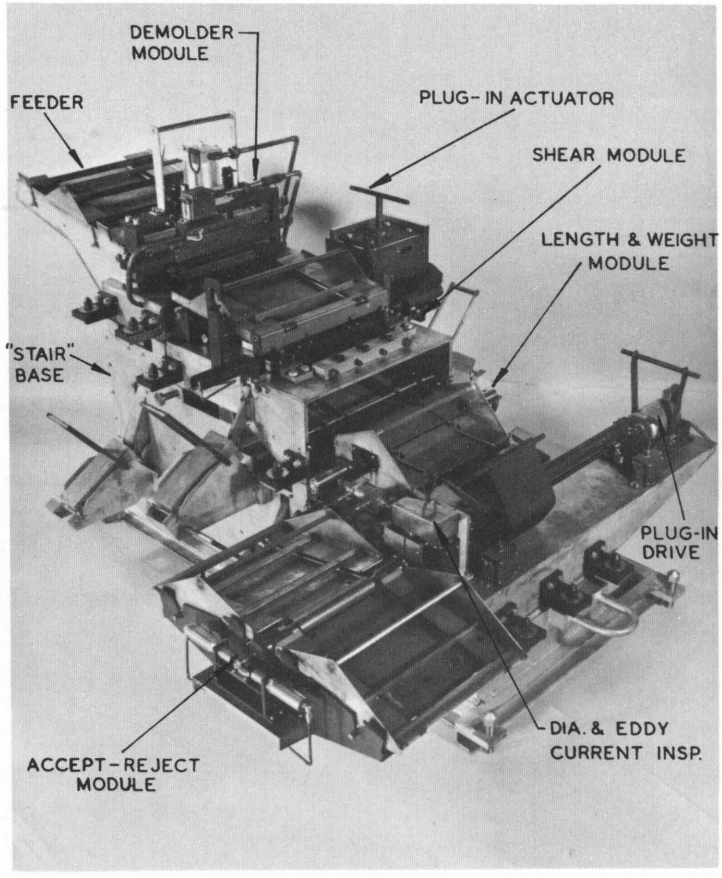

Figure 6. Pin-processing Machine

The remotely controlled work station for preparing charges for injection-casting furnaces is shown in Figure 7. The station consists of an inverter for the container used in transferring melt-refined billets, a crucible positioner and heel extractor, and manipulator tongs for the crucibles and billets.

A master-slave manipulator work station (see Figure 8) was designed and constructed to load Vycor molds into the injection-casting furnace pallet and to force-cool the castings while being unloaded from the pallet into feeder magazines for the pin process machines. Only minor adjustment of this equipment was required. A radiation-resistant blower will be supplied when it is received from the vendor.

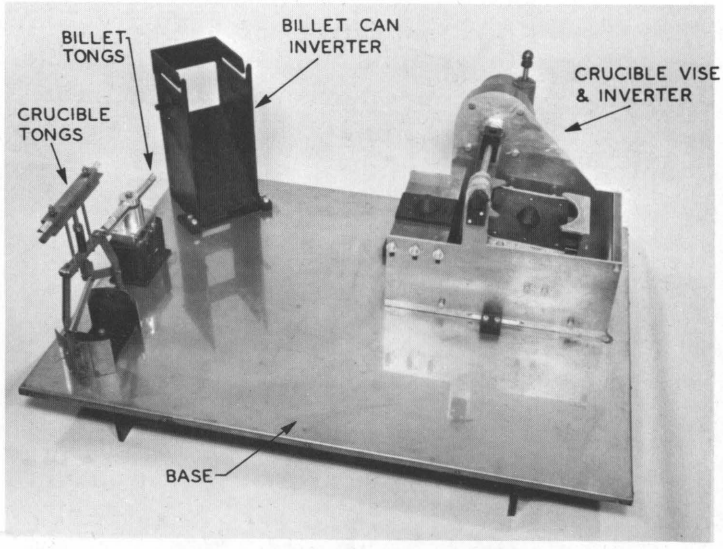

Figure 7. Work Station for Preparing Charges for Injection Casting Furnaces

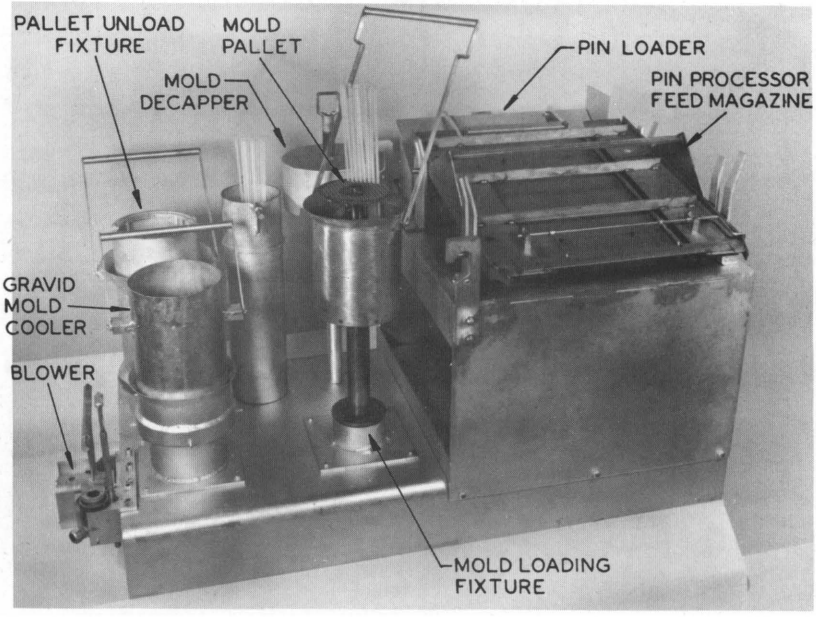

Figure 8. Vycor Mold-loading Station

A manipulator station (see Figure 9), in which the fuel rods will be assembled, was designed, constructed and tested. This equipment is used with a sealed master-slave manipulator to open the sealed container of sodium-filled jackets, to load the jackets into the welder magazine, and to insert fuel pins into the jackets.

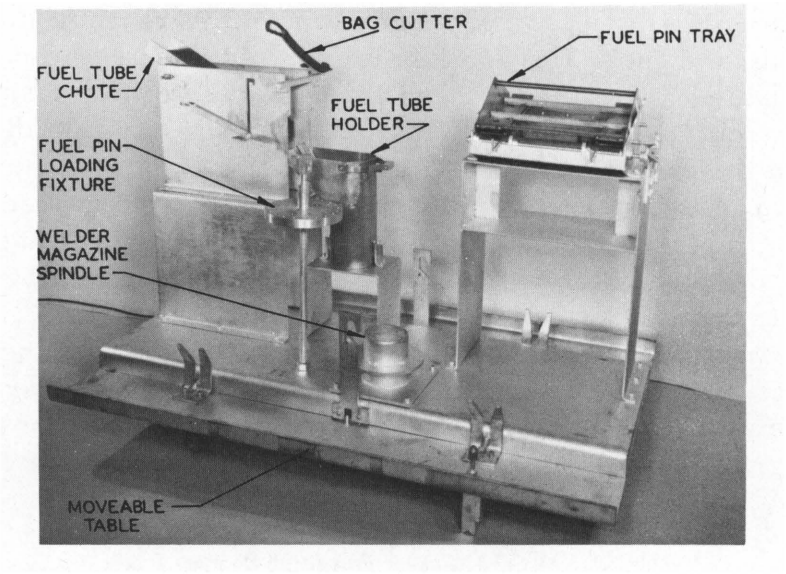

Figure 9. Fuel-pin Loading Station

The settlers have been installed by remote methods, and remote operation of the vibratory motion is complete. The components of the pin-processing machine have been degreased and motion-tested in the mockup area.

The pallet-load station, the furnace-charge table, and a pin-processing base have been transferred into the Argon Cell by remote operating procedures.

The decanner was relocated to eliminate potential interference between the electromechanical manipulators and the sealed master-slave manipulators. This will permit effective utilization of the master-slave manipulators on the decanner.

The melt-refining furnace has been used to melt and cast a low-melting trial alloy successfully.

Equipment for the determination of carbon in steel (used for the carbon-in-sodium program) has been installed and tested. An induction furnace was used for sample ignition followed by measurement of the liberated CO_2 by a differential freeze-out manometer technique.

The possibility that an alloying reaction might occur when declad sodium-coated fuel pins from spent EBR-II fuel subassemblies are brought in contact with stainless steel container vessels was investigated further (see Progress Report for March 1963, ANL-6705, p. 22). One experiment was performed in an argon atmosphere containing 3 ppm water and 3 ppm oxygen under conditions which simulated the handling of declad sodium-coated

fuel pins in the EBR-II fuel-pin charger and in the storage container. In this experiment, the fuel pins after being coated with sodium were placed in a stainless steel (Type 304) box with a removable cover and then heated to 300°C. The sodium coating evaporated from the pins in about 3 hr and redeposited on the inside surface of the box cover. In another experiment, the fuel pins after being wetted with sodium were first stored for 14 hr at ambient room temperature in an argon atmosphere containing 100 ppm of oxygen and 40 ppm of water. The coated pins were then heated for 4 hr at 300°C in the covered stainless steel box. At the end of this time, elemental sodium had evaporated from the fuel pins, but a white coating of sodium oxide and sodium hydroxide was left on the pins. No alloying of the fuel pins with the stainless steel was observed in these experiments. These results are in agreement with earlier results (see Progress Report for March 1963, ANL-6705, p. 22).

Design and installation drawings have been completed for the following equipment items: (1) storage racks for holding four fuel subassemblies or four control subassemblies in each of four storage pits in the floor of the Air Cell (see Progress Report for March 1963, ANL-6705, p. 22), (2) a filter to remove oil which is entrained in the off-gas from the vacuum pumps for the melt-refining furnace, and (3) a prefilter assembly which will be installed on the face of the exhaust duct in the transfer cell.

Shielding sleeves have been installed and seal welded in the penetrations through the wall of the Argon Cell for installation of Model "A" manipulators. Leak testing of the seal welds has been scheduled.

Corrective work is being carried out on the cranes in the Air Cell and the Argon Cell. This work includes: (1) the installation of new supports and insulators for the bus bar collectors (see Progress Report for November 1962, ANL-6658, p. 23), (2) the installation of new bridge drive gear-reducer units (see Progress Report for September 1962, ANL-6619, p. 20), and (3) minor mechanical and electrical modifications.

Silver-molybdenum disulfide brushes will be used to replace the copper brushes that are now being used with the center slip rings in the Argon Cell. These slip rings and brushes, which provide power and control to the cranes, have become scored. The scoring may have occurred during recent air-inleakage tests when the Argon Cell contained a dry, inert gas (nitrogen) atmosphere (see Progress Report for March 1963, ANL-6705, p. 21). The silver-molybdenum disulfide is more suitable for service in a dry atmosphere.

5. Training

Systems training continued with 84 classroom hours being spent by reactor operator trainees in preparation for wet critical and approach-to-power operation.

6. Fuel Development

a. Fuel-jacket Development. Tubing of three of the four niobium-base alloys mentioned in the Progress Report for February 1963, ANL-6698, p. 20, has been sized, finished and annealed. The Nb-5 w/o Zr (D-14), Nb-10 w/o Ti-5 w/o Zr (D-36), and Nb-33 w/o Ta-1 w/o Zr tubes are currently being radiographed and eddy-current inspected, after which they will be delivered for irradiation testing.

Completion of Nb-10 w/o W-10 w/o Ta tubes has been delayed pending the receipt of suitable mandrel stock. Rod stock of 0.210-in. diameter has been fabricated from each alloy for end plug material.

b. Properties of Uranium-Plutonium-Fizzium. Table II shows the data obtained from a series of tests of the tensile properties of a U-10 w/o Pu-10 w/o Fz alloy at various temperatures up to 700°C. The tensile strength varies from 47,700 psi down to 4,300 psi. The maximum strength occurred at 300°C and the minimum at 701°C. The anomalous variation of strength is attributed to the behavior of retained γ phase at room temperature. At 300°C, time is sufficient to transform as-cast specimens to low-temperature phases, which appear stronger.

Table II. Tensile Properties of U-10 w/o Pu-10 w/o Fz Alloy at Elevated Temperatures

Temperature (°C)	Tensile Strength (psi ±1%)	Yield Strength (0.2% Offset)	Modulus of Elasticity (10^6 psi)	Remarks
23.0	33,680[1]	-	12.9	Less than 0.2% fracture strain. Retained γ phase.
300.5	47,720	-	9.7	Less than 0.2% fracture strain. Transformed from γ phase.
501.0	31,840	-	7.3	Less than 0.2% fracture strain. Transformed from γ phase.
701.5	4,360	2,920	6.5	Elongation 9.3%, reduction of area 3.2% in γ phase

[1] Last digits retained for comparison use only.

A specimen heat treated at 500°C for the duration of a test at that temperature (approximately 6 hr at temperature) was tested at room temperature. The specimen was so brittle it shattered in the threaded portion before any results could be obtained.

Ductility in the specimens is low. Only in the γ-phase temperature range could an appreciable elongation be measured.

c. Uranium-Molybdenum Alloys. Success in rolling U-14 w/o Mo at 1050-1100°C reported earlier (see Progress Report for March 1963, ANL-6705, p. 23) had been achieved with initial light reduction of 3 to 4% followed by successive heavy reduction up to 16% per pass.

Further work has shown that the as-cast alloy can withstand normal designed reductions of 14 to 16% per pass at 1050-1100°C without failure.

Trials at lower temperatures down to 950°C were successful with 11 to 13% per pass reduction with a total of 30% reduction.

d. Fabrication of Plutonium-containing EBR-II Test Rods. Present schedules call for irradiating approximately 250 fuel pins of the Th-U-Pu EBR-II type, which are 0.144 in. in diameter as cast. To meet the need for pins, over 150 pins of U-Pu-Fs and Th-Pu alloy compositions have been cast to date, and a total of 400 pins will be made to provide comparison specimens of each type for evaluation and for follow-up irradiation.

The U-Pu-Fs and U-Pu-Fz (containing zirconium) alloys appear to cast similarly to U-Fs and U-Fz, although miscast pins are somewhat more frequent. This appears due to the increased dross on the plutonium alloys. This dross forms a crust in some melts that has prevented mold filling.

Thorium-15 w/o Pu and Th-20 w/o Pu alloys were castable in Vycor molds. An attempt to melt Th-10 w/o Pu resulted in failure of an uncooled induction coil. It is expected that this alloy will have to be fabricated by rolling and swaging because it melts at too high a temperature to be cast in Vycor molds.

The above-mentioned fuel pins will be bonded in jackets of niobium alloy, of vanadium, and of other refractory jacket materials as these become available. Welding tests have been made with Nb-1 w/o Zr alloy tubing. Considerably more current is required to weld the niobium alloy than for stainless steel or Zircaloy. Chills were required very close to the weld bead to control grain growth in the heat-affected zone. The welding controls were rebuilt to provide a stepless weld extinguishing taper.

The assembled fuel rods are to be incorporated in sodium-bonded Type 304 stainless steel secondary capsules. A vanadium-barrier thimble will also be incorporated in some capsules. The EBR-II sodium extruder was redesigned to allow extrusion of larger bars of sodium. A sodium-dedrossing furnace and hot trap has been designed to lower the oxygen in commercial sodium before using it in the fuel elements and capsules.

7. Process Development

a. Melt-refining Process Technology. In the EBR-II melt-refining process, it is expected that fission product iodine will condense, probably as cesium iodide, on the Fiberfrax cover over the melt-refining crucible. However, some of this iodine might be released to the argon atmosphere of the Argon Cell upon opening the melt-refining furnace. A laboratory-scale experiment was performed to obtain data that would allow an estimate to be made of the amount of iodine that might be released to the cell atmosphere.

In this experiment, plant conditions were simulated as closely as possible. A sample of about 20 g of uranium-fissium alloy, spiked with inactive cesium, sodium, and uranium tri-iodide, was irradiated for 48 hr in a thermal flux of about 2×10^{12} n/(sec)(sq cm) and then cooled for 20 days to allow the shorter-lived iodine activities and the 30-hr tellurium parent to decay. The alloy was then heated to 1400°C and held at this temperature for one hour under an argon atmosphere. A Fiberfrax plug was located above the melt and had the same temperature gradient (temperatures of about 1000°C at the bottom and 540°C at the top) that is expected in the Fiberfrax fume traps which will be used in plant melt-refining operations. After the one-hour heating period, the furnace was allowed to cool to room temperature and the system evacuated to remove the radioactive xenon and krypton fission products. The Fiberfrax plug was then reheated to a gradient of 315 to 680°C in one case and to 110 to 150°C in another to simulate two conditions of fission product decay heating. [These two conditions are (1) heating of the fume trap, after the melt is poured, by fission products contained in the skull and the fume trap, and (2) heating of the fume trap, by fission products contained in it, after the fume trap is removed from the melt-refining crucible.] During reheating, iodine released from the Fiberfrax plug was swept out of the system by a stream of argon gas which was then passed through an assembly consisting of charcoal traps and AEC filters. It was found that the iodine activity was released from the Fiberfrax at a nearly constant rate, and that the release rate was much greater (although it was still low) at the higher temperature. After 33 hr at 315 to 680°C, the total quantity of iodine-131 retained by the charcoal filter assembly was about five percent (50 μc) of that present in the Fiberfrax at the start of reheating.

b. Skull-reclamation Process. The skull-reclamation process is under development for the recovery of skull material remaining in a zirconia crucible after melt refining. To remove the skull from the crucible, it is necessary to oxidize the skull, which is thereby converted to a free-flowing powder. It is desirable that removals of greater than 99 percent of the uranium from the crucibles be achieved in routine operations. Three crucibles were pulverized and sampled, after the oxidized skulls had been removed, in order to determine their residual uranium contents. The percentage of uranium remaining in the crucibles ranged between 0.7 and 2 percent of the uranium present in the original skull material.

Process operations were continued in the recently completed large-scale (2.5 kg of skull oxide) integrated equipment for the skull-reclamation process. In this process, a uranium-zinc-magnesium product solution, obtained by reduction of skull oxide, is transferred to a beryllia crucible in which two successive uranium precipitations are performed for purification and concentration of the uranium. These precipitation steps have been performed in two large (12-in. O.D. by 20 in. high), thixotropically cast beryllia crucibles, the first of this size to be evaluated. Unlike the small beryllia crucibles that were used in previous tests, the large crucibles were wet by the magnesium-zinc solutions, making it impossible to remove the uranium product concentrate. Since nonwetting of the crucibles is relied upon to permit removal of the uranium product, an inquiry was made to determine the cause of the unexpected behavior encountered in the use of the large crucibles. It was learned that gas firing had been used in the manufacture of the large crucibles, whereas the previously obtained small crucibles had been electrically fired. Large electrically fired beryllia crucibles will be ordered to determine if this difference in manufacturing procedure is responsible for the difference in behavior of the crucibles.

The effect of the presence of components of stainless steel on the skull-reclamation process is being studied to determine whether this process is capable of handling fuel pins which cannot be declad because of deformities. Chromium is the only troublesome constituent (see Progress Report for April 1962, ANL-6565, p. 26) of stainless steel, since it is partially extracted along with uranium from the zinc solution into the flux phase on oxidation of uranium with zinc chloride.

In a recently completed run, about 20 g of stainless steel-clad 5 w/o fissium-uranium fuel pins was dissolved in 200 g of zinc at 750°C under argon and then the solution was contacted with 200 g of flux (44.1 m/o calcium chloride, 44.1 m/o magnesium chloride, 4.6 m/o magnesium fluoride, 7.1 m/o zinc chloride). The flux phase was separated from the zinc and then contacted with another 200 g of zinc. After the two extractions were made, it was found that about 99 percent of the chromium originally present had been removed from the system. However, material balances were unsatisfactory, and it is now believed that other mechanisms besides extraction may be involved in the removal of chromium. Further studies of chromium removal are being planned.

c. Materials and Equipment Evaluation. In an effort to obtain a measure of the reliability of tungsten and a 30 w/o tungsten-molybdenum alloy as containment materials for zinc halide flux systems, corrosion testing has been carried out at 1000°C, which is 200°C higher than used in the process. After 500 hr at 1000°C, it was found that pressed and sintered tungsten had been attacked intergranularly to a depth of 2 to 4 mils and that arc-cast molybdenum-tungsten alloy was attacked to a depth of 2 to 8 mils. Grain sizes were not greatly affected. Sharp edges remained on the

specimens, and dimensional changes were less than one percent. These are considered to be satisfactorily low corrosion rates for the EBR-II fuel-recovery processes now under consideration.

A series of experiments is in progress to determine the effect of small amounts of added impurities on the stability of uranium in magnesium-zinc solutions. Two experiments have been completed in which additions of silicon or stainless steel were made to agitated uranium solutions contained in a pressed and sintered tungsten crucible at 800°C. Although analyses are still incomplete, available results show that additions of 0.05 to 1 w/o silicon caused uranium to precipitate from a magnesium-zinc solution containing 4 w/o uranium. The addition of one w/o silicon to the 4 w/o uranium solution reduced the uranium concentration to 0.02 w/o. Stainless steel had no effect up to a concentration of 0.1 w/o, but at a concentration of 2 w/o, it caused a decrease of about 5 percent in the uranium concentration.

D. FARET

1. Construction Program

The study to determine design feasibility and to estimate cost and schedule for the construction of FARET is complete. This study was performed by Atomics International, Inc., and Shaw Metz and Associates, in conjunction with the Laboratory. The final report will be issued next month. The basic concept of FARET is now established and its design feasibility is determined. The design described in the study report is essentially that previously presented (see Progress Report for February, 1963, ANL-6698, p. 24; an error in Figure 3, wherein cell and vault nomenclature were reversed should be noted). The estimated cost of the facility is $17,000,000, and the engineering and construction schedule is 42 months, exclusive of checkout and startup.

A number of important matters have been resolved during this period. The board for the selection of an architect-engineer has completed its work, and a recommendation has been made to the Commission. An architect-engineer procedure manual has been completed and submitted to the Commission for approval. A site request letter has been submitted to the Commission requesting approval of the site located about 4000 ft southeast of EBR-II.

2. Reactor Model

A full-scale model of the top ends of the FARET subassemblies and of the reactor vessel at that elevation has been constructed (see Figure 10). This model is being used to facilitate visualization of various core configurations and the positions of different control rods. Several methods for passing instrumentation cables from the subassemblies to the outside of the reactor vessels will be tried out with the aid of this model.

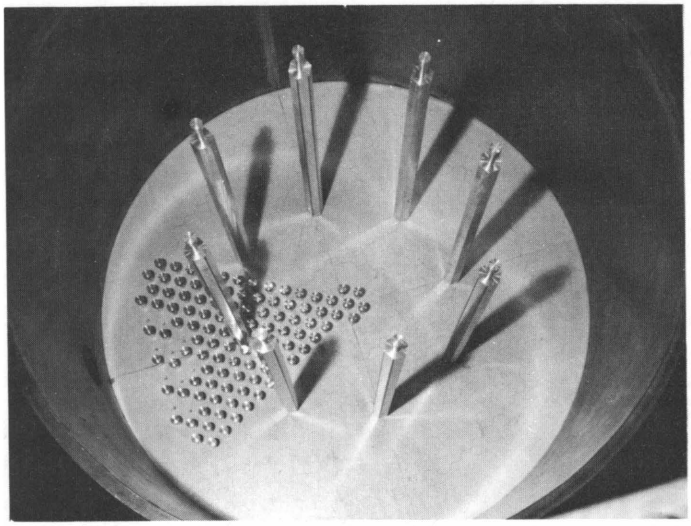

Figure 10

Full-scale Model of Top of FARET Sub-assemblies and Reactor Vessel

3. Model Fuel Element (Zoned-core Test Zone)

Work has continued on the development of a fuel element which will permit measurements of the fuel temperature coefficient to be made with FARET. The element consists basically of fuel pellets which are segmented, to reduce overall fuel expansion, and insulated from the cladding, to make it easier to obtain large fuel temperature changes with little or no change in the temperature of coolant and structure. Various methods of maintaining an insulating gap between pellets and clad, and of supporting the segmented pellets on the clad, are being considered. Table III illustrates and describes these methods and discusses their relative merits; Table IV lists pertinent properties of the structural materials which may be used in the fuel element. (It should be noted that in Table IV, some interchangeability between the separator concepts and the fuel pellet-clad concepts is possible.) Work being done on the actual development of concept No. 1, Table III, is described in the Progress Report for December 1962, ANL-6672, p. 22 and in Progress Report for March 1963, ANL-6705, p. 29. Procurement of parts to permit active development of concepts No. 2 through 4 and No. 8 has begun.

4. Sodium Cleanup

Work has started on the modification of an existing small sodium loop to conduct studies of hot trapping. Gettering ability of some unconventional materials, including some that might be used for cladding, will be studied. Among these are manganese, niobium, tantalum, and vanadium, all of which are thermodynamically capable of reducing sodium oxide.

The possibility of employing a distillation type of system for sodium purification in FARET is being investigated. During FARET operation at coolant temperatures above 800°F, hot trapping will be employed. Unfortunately, this method of purification is limited to the removal of oxygen

Table III. Various Fuel Separator Concepts

FUEL PELLET	CLAD	SEPARATOR	REMARKS
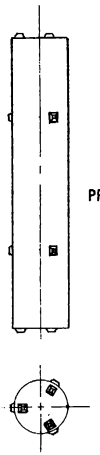 WITH INTEGRAL PROJECTIONS	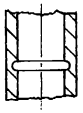 GROOVED BORE MIN. THK. 0.045 in.	① 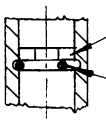 THORIA SUPPORT WASHER RETAINING SPRING	CURRENT REFERENCE. EASILY ASSEMBLED & DISASSEMBLED. DUE TO LIMITED CONTACT OF RETAINING RING TO CLAD, MODEL IS RESTRICTED TO LOWER TEMPERATURE EXPERIMENTS. REQUIRES THICK TUBING (6.4% F.V.R.)*
	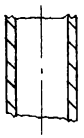 SMOOTH BORE	② 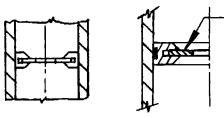 TUNGSTEN SUPPORT WASHER & INTEGRAL RETAINING RING (BRAZED TO CLAD)	OCCUPIES LEAST VOLUME. HIGH MELTING POINT OF TUNGSTEN AND GOOD THERMAL CONDUCTIVITY OF NICKEL SHOULD MAINTAIN INTEGRITY AT HIGH TEMPERATURE. (NO MODEL TO DATE) (3.5% F.V.R.)*
		③ 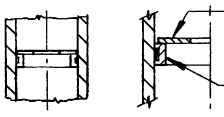 TUNGSTEN SUPPORT WASHER (LOOSE) RETAINING RING (BRAZED TO CLAD)	ALTERNATE TO #2. PROBABLY SIMPLER TO FABRICATE (NO MODEL TO DATE) (5.0% F.V.R.)*
		④ 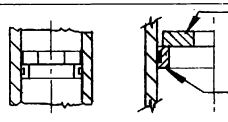 THORIA SUPPORT WASHER RETAINING RING (BRAZED TO CLAD)	ALTERNATE TO #2 OR #3, IF NICKEL RING REQUIRES TO BE INSULATED (NO MODEL TO DATE) (6.5% F.V.R.)*
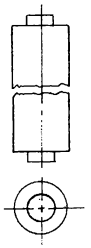 WITH LOCATING ENDS	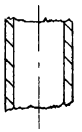 SMOOTH BORE	⑤ 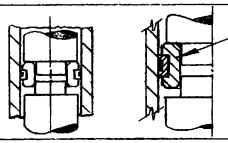 THORIA SUPPORT WASHER WITH INTEGRAL RETAINING RING (BRAZED TO CLAD)	SUPPORT WASHER INSULATES RETAINING RING AND BRAZED JOINT. IF WASHER SHOULD CRACK, DESIGN TRAPS FRAGMENTS AND SUPPORTS PELLET (NO MODEL TO DATE) (6.0% F.V.R.)*
		⑥ 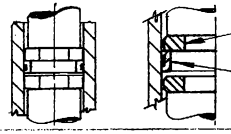 THORIA LOCATING WASHER (LOOSE) SEPARATE RETAINING RING (BRAZED TO CLAD)	ALTERNATE TO #5 (NO MODEL TO DATE) (6.5% F.V.R.)*
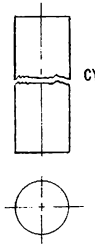 PLAIN CYLINDER	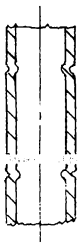 WITH INTERNAL PROJECTIONS	⑦ 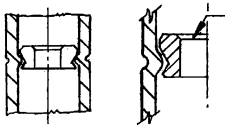 TANTALUM OR TUNGSTEN SUPPORT WASHER SNAPPED INTO PLACE	ONE MODEL MADE FOR TWO PELLETS. EASILY ASSEMBLED AND DISASSEMBLED. GOOD PELLET SUPPORT AND ACCURATE BOND SPACING. HIGH THERMAL CONDUCTIVITY OF TANTALUM OR TUNGSTEN AND LIMITED CONTACT OF SUPPORT WASHER TO CLAD. REQUIRES BENCH TESTING (5.5% F.V.R.)*
		⑧ 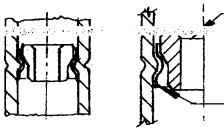 THORIA SUPPORT WASHER FORMED TANTALUM RETAINING RING	ALTERNATE TO #7, IF INSULATION IS REQUIRED (8.0% F.V.R.)*

*F.V.R. "FUEL VOLUME REDUCTION"

Table IV. Fuel Separator Materials - Related Physical Properties

MATERIAL	MELTING POINT (°C)	THERMAL CONDUCTIVITY* [w/(cm²)/(°C)/(cm)]	LINEAR COEFFICIENT OF THERMAL EXPANSION (10^{-6}/°C)	TENSILE STRENGTH* (psi)	REACTION WITH UO_2 (°C)	USE	REMARKS
AISI 316 STAINLESS STEEL	1400	0.16	17.2	90,000	750	CLAD	COMPATIBLE WITH SODIUM
						RETAINING RING	LOW THERMAL CONDUCTIVITY AND MELTING POINT. RING MAY REQUIRE TO BE INSULATED
NICKEL "A"	1425	0.62	16.9	65,000	1370	RETAINING RING	GOOD THERMAL CONDUCTIVITY. RING MAY NOT REQUIRE TO BE INSULATED IF BRAZED TO CLAD
THORIA (ThO_2)	3300	NEGL.	9.5	20,000	--	SUPPORT WASHER	POOR DUCTILITY HIGH MELTING POINT LOW THERMAL CONDUCTIVITY GOOD INSULATOR
TANTALUM (Ta)	3000	0.55	6.5	60,000	1250	SUPPORT WASHER	HIGH MELTING POINT INDICATES USE WITHOUT INSULATOR. EASY TO FABRICATE (MUST BE USED IN INERT ATMOSPHERE OR VACUUM)
TUNGSTEN (W)	3400	1.67	4.4	220,000	NONE	SUPPORT WASHER	HIGH MELTING POINT INDICATES USE WITHOUT INSULATOR. DIFFICULT TO FABRICATE (MUST BE USED IN INERT ATMOSPHERE OR VACUUM)
UO_2	2170	0.11	8.0	13,000	--	FUEL	

* AT ROOM TEMPERATURE

and possibly of nitrogen and carbon. Other impurities and corrosion products would remain in the coolant and continue to build up. By supplementing the hot trapping with a distillation type of purification system, separation of all contaminants should be possible except for potassium and cesium, which distill over with the sodium. Preliminary studies show that the surface area provided by a still 90 cm in diameter could provide evaporation rates of ~100 kg/hr. If it be assumed that complete purification of the distillate can be obtained and that the distillate is cycled back to the main body of sodium (8000 gal) a 40% reduction in the impurity level would result after one week of operation.

5. In-vessel Electrical Connectors

In-vessel electrical connectors for operation up to 650°C appear to be commercially available. Specifications are now being written and a sample lot will be purchased from the manufacturer.

An experimental program for testing these connectors is being formulated. The tests will be conducted in a sodium vapor-argon atmosphere which will simulate the actual condition of reactor operation. The insulation and contact resistance, as well as the integrity of the connector, will be measured from room temperature up to 650°C. Changes in these parameters will be studied as a function of the number of times a connector is used.

6. Fuel-pin Temperatures

It is necessary to develop thermocouples which are capable of operating at the temperatures and environment of a fuel pin. It appears that thermocouples made of tungsten-5% rhenium vs. tungsten-26% rhenium will satisfy the temperature requirements.

A theoretical analysis is being made of the relationship of the insulation resistance and capacitance of coaxial and two conductor cables on the performance of the thermocouple. These calculations are necessary to determine the optimum size of diameter for the thermocouple wire and the wire spacing in a sheath of a given diameter. It will also show whether there are any advantages of using a coaxial type of cable for thermocouples.

A literature search has been made to determine the compatibility of some of the materials that are considered potentially useful for thermocouples. It has been found that both tantalum and tungsten do not react with uranium dioxide at 2760°C in an argon atmosphere at a pressure of 20 to 37 mm of mercury. This means that either material can be used as a sheath for a thermocouple. It has also been found that thoria (ThO_2) is stable with tantalum up to 2795°C and with tungsten up to at least 2645°C This means that thoria can effectively be used as an electrical insulator providing its electrical conductivity is low enough.

The published values for the electrical conductivity of thoria are not in good agreement and do not go above 2000°C. The poor agreement appears to be due to the purity of the ThO_2. Small amounts of CeO_2, Y_2O_3, or La_2O_3 tend to increase the conductivity appreciably. Contaminants such as magnesium and aluminum are also to be avoided because thoria is reducible in their presence at high temperature, causing an increase in conductivity. Unless some new data are found, it may be necessary to determine these values for ThO_2 experimentally.

III. GENERAL REACTOR TECHNOLOGY

A. Applied Nuclear Physics

1. Scattering of Fast Neutrons from U^{238}

The experimental study of scattering from U^{238} is now essentially complete. A summary of the results is given in Figures 11 and 12, which indicate the elastic and the inelastic scattering cross sections of U^{238}, respectively.

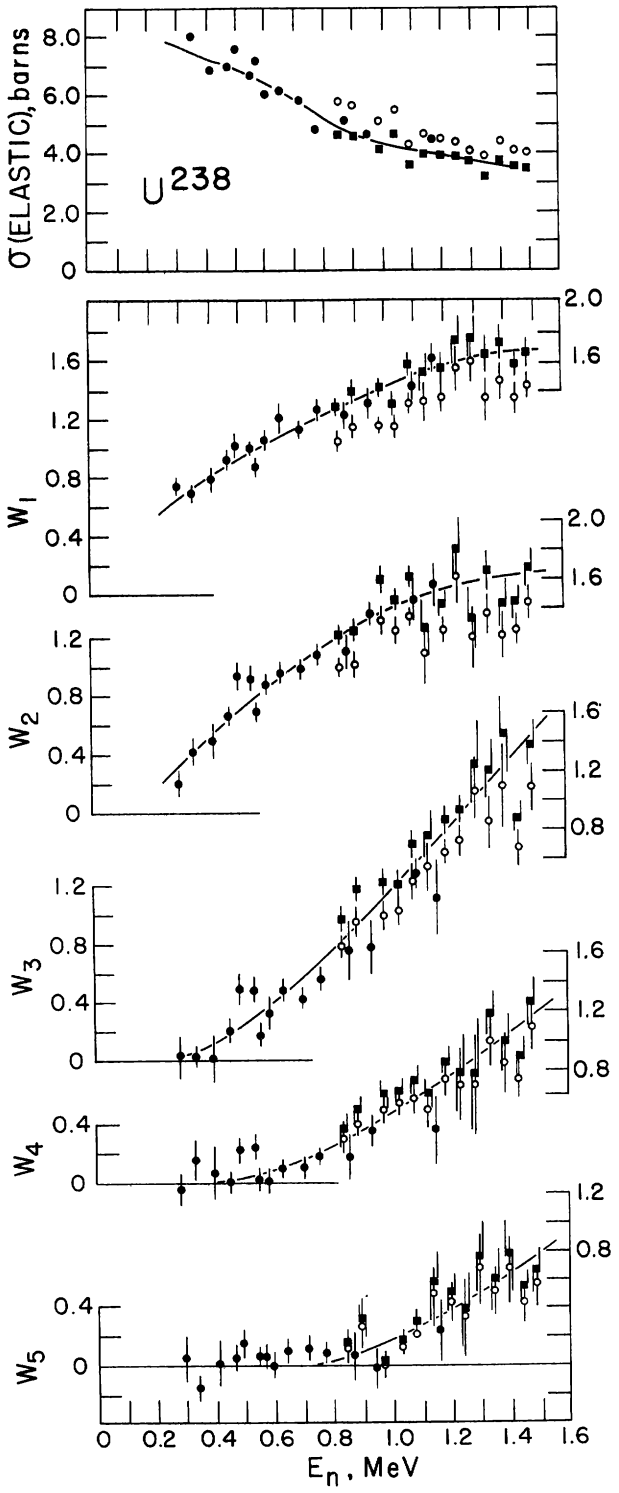

Figure 11. The Elastic Cross Section of U^{238} Expressed in the Form $\frac{d\sigma}{d\Omega} = \frac{\sigma}{4\pi}\left[1 + \sum_{i=1}^{5} W_i P_i\right]$

The elastic and inelastic scattering of fast neutrons from natural uranium was studied throughout the incident neutron range from 0.3 to 1.5 Mev. Time-of-flight techniques were utilized to determine the energy spectrum of scattered neutrons. The differential elastic-scattering cross section was determined at incident neutron energy intervals of $\lesssim$50 kev. The cross sections for the inelastic excitation of residual nuclear levels at 45 ± 3, 150 ± 5, 630 ± 20, 720 ± 20, 930 ± 30, 1000 ± 30, and 1050 ± 30 kev were measured. The differential cross section for inelastic scattering to the 45-kev level was essentially symmetric about 90°. The remaining inelastic groups were emitted isotropically. All cross sections were determined relative to the known elastic-scattering cross section of carbon. The experimental results were compared with the Hauser-Feshbach theory and possible evidence for direct interaction processes was assayed.

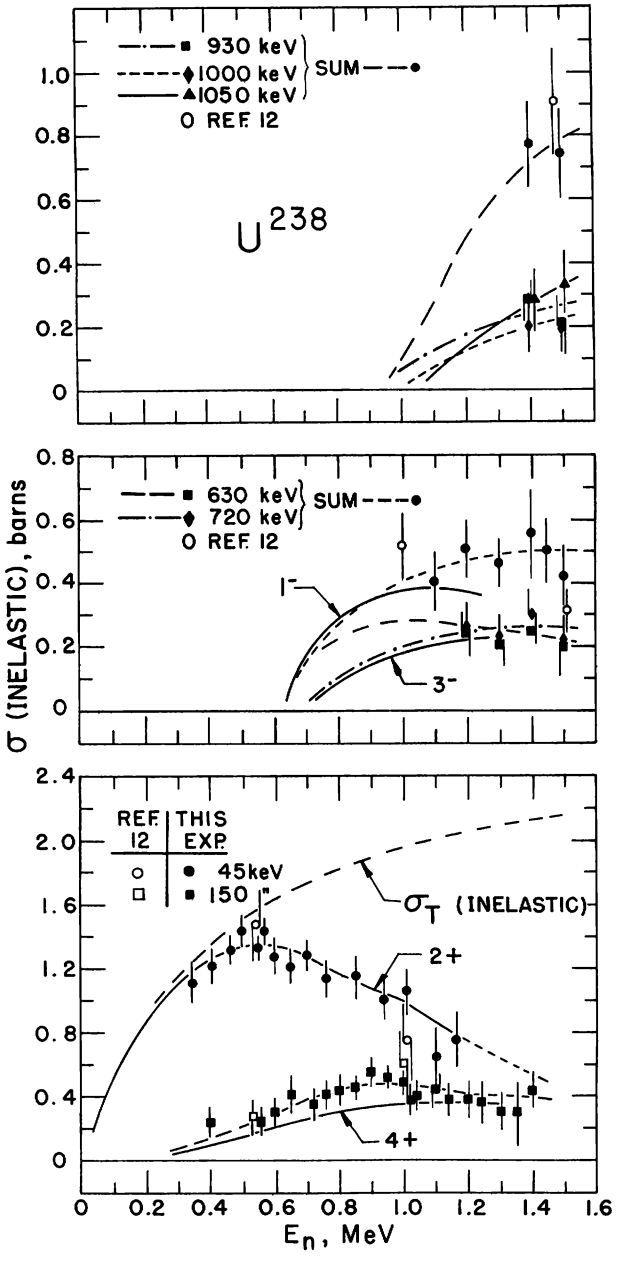

Figure 12. The Inelastic Cross Section of U^{238}

The above results, to a considerable extent, satisfy reactor requests for nuclear data.*

2. Scattering of Fast Neutrons from Ta^{181}

Periodically, the status of the experimental measurement of scattering from Ta^{181} has been given. This work is now complete and is summarized below.

The spectrum of neutrons scattered from Ta^{181} was measured at incident neutron energies from 0.3 to 1.5 Mev. Time-of-flight techniques were employed to resolve the elastically and the inelastically scattered components. The angular distribution of the elastically scattered neutrons was measured at $\lesssim$50-kev intervals with an incident neutron-energy spread of ~20 kev. Inelastically scattered neutron groups resulting in the excitation of residual nuclear levels at 140 ± 10, 300 ± 10, 620 ± 20, 725 ± 25, 900 ± 30, and 980 ± 30 kev were observed. The measurements indicated that the levels at 725 and 980 kev were composed of two or more components. In addition, inelastic scattering to a (480 ± 20)-kev level was tentatively observed. The magnitudes of the differential elastic cross sections and of the inelastic excitation functions were determined relative to the known elastic-scattering cross section of carbon. The experimental results were compared with those obtained in previous measurements and a qualitative comparison was made with theoretical calculations.

The results of the elastic and inelastic measurements are graphically shown in Figures 13 and 14, respectively. These results are particularly useful in carrying out the physics analysis of high-temperature reactor systems which contain appreciable quantities of tantalum.

*See the Compilation of Requests for Nuclear Data prepared by ACRP, NCSAG, and EANDC.

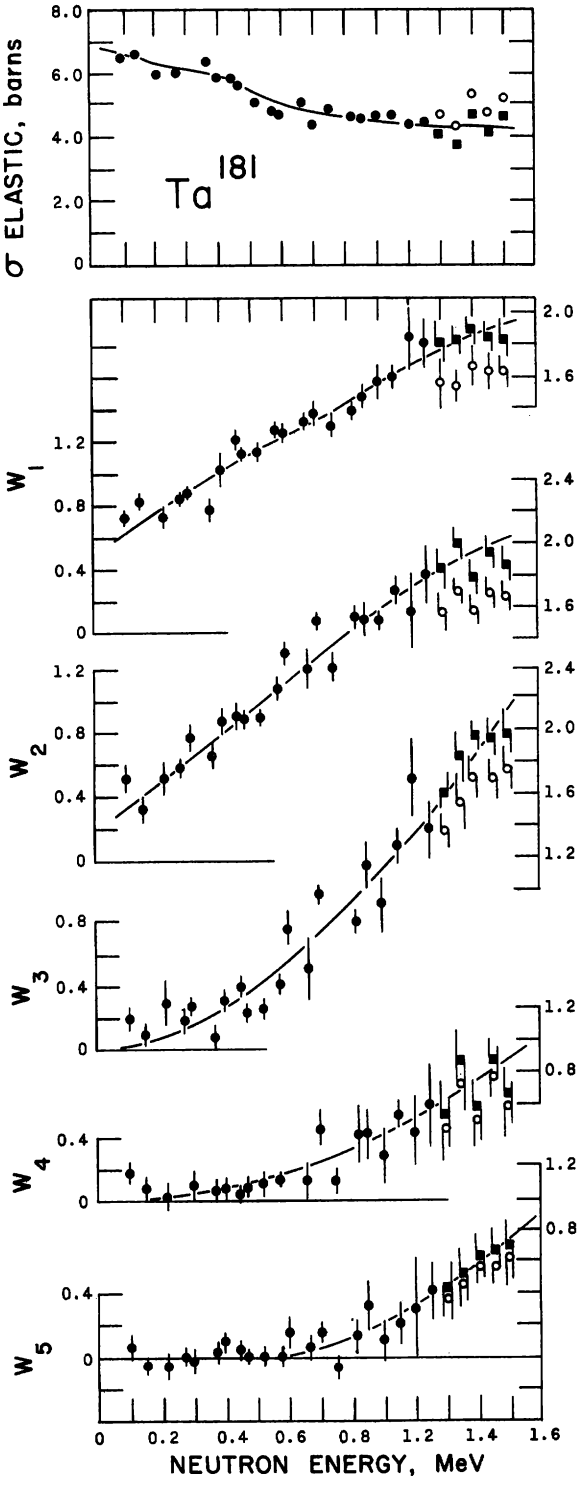

Figure 13. The Elastic Scattering Cross Section of Ta^{181} Expressed in the Form

$$\frac{d\sigma}{d\Omega} = \frac{\sigma}{4\pi}\left[1 + \sum_{i=1}^{5} W_i P_i\right]$$

3. Widths of Single-particle Bound States (Theory)

Recent high-resolution experiments on deuteron stripping and gamma-ray scattering have suggested the possibility of determining, not only the energies of single-particle bound states, but also their widths. Such widths can be related to the imaginary part V_I of the optical-model potential used in the description of single-particle unbound states to show that the measurements of such widths can be of considerable importance to the determination of the spatial distribution of V_I and the magnitude of the rearrangement energy Δ. These quantities are of considerable importance in understanding nuclear reactions including those induced by fast neutrons.

4. Neutron-capture Cross Sections

For some time we have been concerned with the large differences which exist in the absolute values of neutron-capture cross sections. In the incident neutron-energy range above approximately 100 kev, the two most widely used methods for determination of both the energy dependence and absolute value of neutron-capture cross sections have been the neutron activation method (measurement of neutron-induced activity) and the large liquid scintillator pulsed source method (measurement of the prompt gamma radiation following neutron capture).

The large liquid scintillator measurements were carried out primarily by Diven et al. at Los Alamos[1] and by Gibbons et al. at

[1] B. C. Diven, J. Terrell, and A. Hemmendinger, Phys. Rev. 120, 556 (1960).

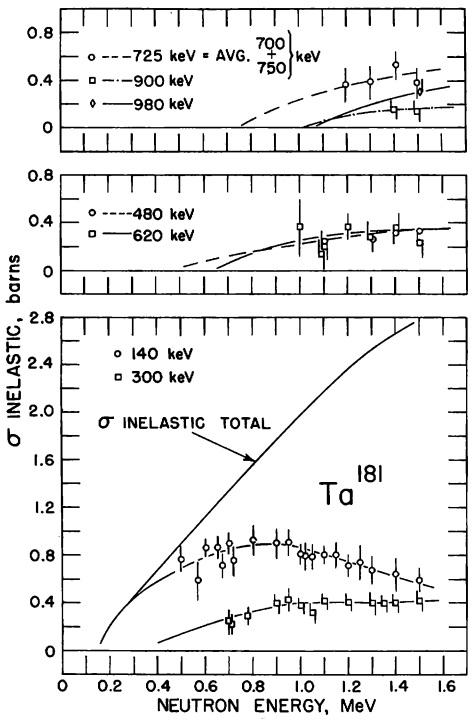

Figure 14. The Inelastic Cross Section of Ta^{181}

Oak Ridge.[2] In both laboratories, the irradiated samples were "natural" elements. Thus, activation results can be directly compared with liquid scintillator results only when the activation cross sections are known for all of the naturally occurring isotopes of a given element and for all of the independent metastable and ground-state decay branches of a given isotope. We have measured the activation cross sections for bromine, rhodium, indium, and iodine. The activation cross sections were combined to form the total neutron-capture cross sections for the natural elements. Our results, together with those of Los Alamos and Oak Ridge, are given in Fig. 15. It is evident from the figure that our results are in good agreement with the Los Alamos results. In the case of indium, some of the difference between our results and those of Los Alamos may be explained by the fact that we did not measure the activation cross section for the 4.3% abundant isotope In^{113}. For the other elements all of the required activation cross sections were measured.

5. High-conversion Critical Experiment

The ZPR-VII facility has been reloaded with Type 6061-T6 aluminum-clad fuel in the 1.24-cm-square lattice pattern. A previous loading with this fuel at the start of the Hi-C program had indicated a clean critical loading of 987 ± 5 fuel pins in a 31 x 33 array of fuel pins. The current loadings indicate a clean critical fuel pin number of 938 ± 2 for a cylindrical, fully water-reflected core.

The finger-rod clusters are worth about 1.7% $\Delta k/k$ each, and the blade rods are worth about 0.7% $\Delta k/k$ each. The fingers are located 12.5 cm from the core center, and the blades are approximately 2 cm from the core boundary. Flux-traverse measurements are now scheduled.

Data obtained from a previous core containing stainless steel clad fuel are being analyzed. The buckling measurements made in the uniform 1.24-cm-square stainless steel Hi-C core have been re-examined in an attempt to establish the asymptotic region of the core. Four radial flux

---

[2] J. H. Gibbons, R. L. Macklin, P. D. Miller, and J. H. Neiler, Phys. Rev. 122, 182 (1961).

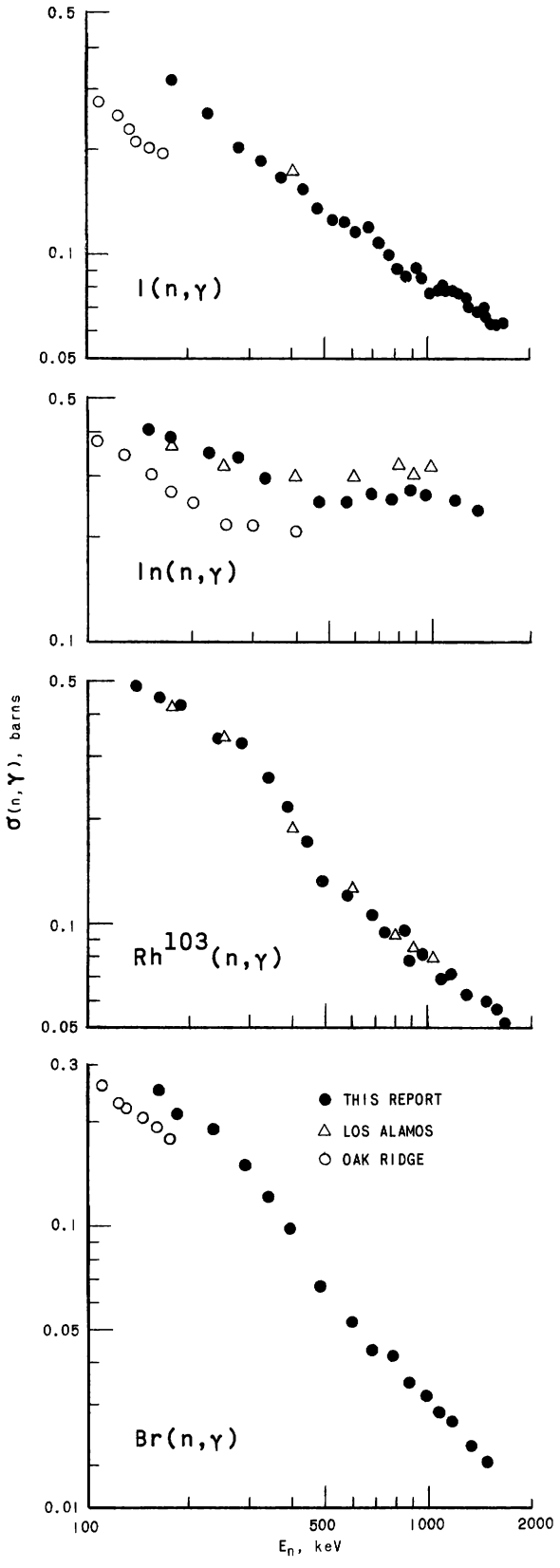

Figure 15. Neutron-capture Cross Sections of Bromine, Rhodium, Indium, and Iodine

traverses were made with each of the following detectors: cadmium-covered gold, cadmium-covered manganese, bare gold, and bare manganese. These 16 traverses were then fitted to J_0 curves for radii of 24.8, 19.8, and 14.8 cm. It was hoped to find the fitting radius out to which the bare and cadmium-covered data gave the same value of B_r. The results, even though marginal, did indicate that the data from cadmium-covered gold and manganese gave the same value of B_r for fitting radii out to at least 25 cm in a core of 29-cm radius. A statistical analysis indicated that the bare data gave a smaller value of B_r than the cadmium-covered data at a radius of 24.8 cm, whereas the bare and cadmium-covered data gave the same B_r values out to fitting radius of 19.8 cm. These differences are ascribed to the boundary effect of the water reflector.

An additional bare gold traverse was taken with more data points inside a radius of 19.8 cm. These data indicated a B_r value equal to that obtained with cadmium-covered foils when the fitting radius was in the range 14.8-19.8 cm. When a fitting radius smaller than 14.8 cm was used, the fitting error became large.

A second set of initial-conversion-ratio (ICR) data was obtained and analyzed for the 1.24-cm-square stainless steel Hi-C core. When analyzed in the customary fashion, the new data gave a value for the ICR that is essentially unchanged from the value of 0.55 reported in Progress Report for March 1963, ANL-6705, p. 34. Nonetheless, examination of the

results obtained with various foils and foil materials has revealed certain systematic discrepancies in the measurements. The two discrepancies result from:

(1) a variation in the fission product correction factor as a function of foil thickness, and

(2) self-attenuation in the foil of the 100-kev γ activity that is of the order of 7% per mil.

The effect of these factors on the ICR is being investigated.

The relatively severe self-attenuation (~30% for a 5-mil foil) has directed our attention to still another systematic effect which may be sufficiently significant to require revision of the ICR values previously reported. This arises from differences in the spatial distribution of the Np^{239} in a foil which is irradiated in a fuel rod geometry and a bare foil irradiated in a thermal flux. As a result there appears to be a significant difference in the overall detection efficiency for the neptunium activity in the two foils. The effect is more severe when the ratio of the epithermal/thermal induced activity (E/T) is large. In the Hi-C fuel, $E/T \sim 4$. In an approximately analogous case in which $E/T \sim 1$, the relative difference in counting efficiencies is reported to require a 6% correction.[3] An experiment to investigate the correction required for the Hi-C fuel foils is being planned.

A second set of data was also obtained for the U^{238} capture cadmium ratio in the 1.24-cm-square stainless steel-clad core. The comments of the previous paragraph are generally also applicable to the cadmium ratio data since the counting techniques are identical.

6. Fast Neutron Spectroscopy

Additional tests have been made with the lithium-sensitized solid-state neutron spectrometers in which high-energy resolution is achieved by providing collimation for the reaction products. Data showing the height distribution of pulses from the lithium spectrometer when exposed to various sources of fast neutron fluxes have become available.

One set of measurements made with a monoenergetic beam from the Van de Graaff accelerator shows the characteristic split in the single triton lines predictable from the center-of-mass motion of the compound nucleus and the angle between neutron beam and counter axis. The peaks in the pulse-height-distribution curves from neutrons of higher energies have shown a displacement linear with energy and well discernible for energies about 200 kev, when seen with a low-resolution, high-sensitivity instrument.

[3] B. Arcipiani et al., A Note on the Measurement of U^{238} Cadmium Ratio, Nuclear Science and Engineering, 14, 316 (1962).

As in similar measurements in the JUGGERNAUT fast converter facility, the thermal and epithermal neutron background has been detected with very great efficiency and forms a prominent broad line corresponding to about zero energy; since the thermalization of room-scattered neutrons is not complete, this line is not representative of the capability of counter resolution.

Measurements of neutron spectra with a coincidence arrangement, by means of a very high-resolution, small-volume, low-sensitivity spectrometer in the grazing hole of the Argonne Fast Source Reactor (AFSR) have shown a widened sum pulse distribution consistent with the neutron-energy distribution expected from the reactor. The reproducibility of the position of the thermal reference line is the major problem at this time. Discounting this limitation, a recent set of data from the AFSR shows quantitatively the performance of the spectrometer in a fast flux. By using the thermal-reference line position and pulse distribution obtained in the AFSR grazing hole, it can be shown that there is a maximum peak in the fast flux at approximately 110 kev, consistent with the results of earlier, conventional flux measurements. A second peak is seen in the pulse-height distribution and corresponds to the position of the resonance in the $Li^6(n,\alpha)$ cross section.

7. Criticality Monitor

The criticality monitor has been modified and reinstalled in the AFSR. A new differential electrometer circuit has been built to read the wheel-of-fortune filter. The new circuit has two pairs of differential pickups oriented 90° apart. The circuit provides amplification, full-wave rectification, and summing of the two differential signals. This provides an improved dc signal proportional to the ac component of the flux signal.

The new circuit has been tried; some instability was noted. The probable cause has been determined and is being corrected.

8. Spectral Information from Foil Irradiations

For assemblies having the high fuel-to-moderator ratios of BORAX-V and Hi-C, it is not unreasonable to predict a flux depression in the energy region of the U^{238} resonances (~0.5 to 150 ev). A plot of GAM-1 epithermal spectrum predictions for Hi-C cores shows, not a $1/E$ pulse with $E\,\phi(E)$ = constant, but rather a spectrum of the form

$$E\phi(E) - E_n\,\phi(E_n) = k\ell n\,(E/E_n) \quad ,$$

where E_n can be any convenient reference energy. There are perturbations due to individual U^{238} resonances, but no $1/E$ region is apparent, even below the lowest U^{238} resonance.

Assuming this same epithermal spectral model, intensive calculations have been made from the cadmium ratios measured in the BORAX-V superheater experiment. It was found that the assumed spectral model is consistent with the data (from indium, gold, manganese, and copper) in the peripheral zone, but that discrepancies appeared in the data taken in the superheater zone: the cadmium ratios for indium and manganese were consistently higher than would be expected on the basis of the results from the gold and copper. It seems that this is due to two effects:

(a) The superheater fuel being highly enriched, the resonance activation of the indium (1.46 ev) is partially shielded by the U^{235} resonances at 1.1 ev and 2 ev.

(b) The superheater assembly contains a large amount of Type 304 stainless steel which, in turn, contains as much as 2% manganese. The resonance shielding of the manganese foils by this manganese is appreciable. A reduction of about 13% in the ratio of epicadmium-to-subcadmium activation is observed in the case of the manganese, and of about 10% in the case of the indium.

9. Theoretical Physics

a. Numerical Methods Analysis. In integrating ordinary differential equations, open integration formulas are needed, which estimate the solution $y(x_n)$ in terms of the derivative y at x_n, and of values of y and y' at x_{n-1}, x, $\cdots$, x_{n-k}. Such formulas are customarily derived by assuming that y may be represented adequately by a polynomial over the range from x_{n-k} to x_n. If the solution is badly behaved, this representation is only adequate with a very short step size and corresponding expense. Many badly behaved functions are far better approximated by ratios of polynomials than by single polynomials. However, open integration formulas have not been developed for this type of approximating function. If the solution is approximated by $(p_0 + p_1x)/(1 + q_1x)$, the resulting integration formula is

$$y_n = y_{n-1} + \left(y'_{n-1}\right) h \sqrt{y'_n\, y'_{n-1}}$$

This formula was tested on the equation $y'(x) = -2xy^2$. The true solution of this is $y = 1/(1 + x^2)$ if $y(1) = \frac{1}{2}$. Using the integration formula, the errors at x = 2 are 3.6% for h = 1, 0.9% for h = 0.5, and 0.086% for h = 0.25. These results are considered encouraging.

b. Doppler Effect Calculations. A new 22-group set of cross sections has been prepared and is now being used in making calculations involving the Doppler effect. Cross sections are available for the following materials: Pu^{239}, U^{235}, U^{238}, Th^{232}, sodium, aluminum, oxygen, carbon, and stainless steel. The upper 11 groups, those above 25 kev, are the same as the Yiftah, Okrent, and Moldauer set except for modifications to $\sigma(n,\gamma)$

cross sections for Pu^{239} and U^{238}. In addition, the transport and elastic-removal cross sections of light elements are not used as all the Doppler effect calculations are done directly with the ELMOE code. In the lower 11 groups, cross sections of fertile and fissile materials have been evaluated as a function of temperature and σ_p, the equivalent elastic-scattering cross section per atom.

For the fissile materials an improved resonance-overlap calculation has been incorporated. This has the effect of reducing the fissile-material Doppler effect by up to about 20%. For Pu^{239}, variations in the strength function, $\langle \Gamma_n^0 \rangle / D$, average fission width, level spacing, and channels per fission have been made to determine the effect on the Doppler coefficient.

Because of the significant contribution of neutrons of intermediate energy, say between 0.5 and 10 kev, to the Doppler effect, an investigation has been made of the Doppler broadening of Pu^{239} and U^{235} resonances in this region. Previous work in this field has been summarized by Nicholson.[4]

A problem arises from the fact that neither Method A nor Method B described by Nicholson is clearly applicable in this intermediate-energy region. Since the level spacings of these fissile materials are relatively small compared with those of fertile material, "Method B," which does not include the overlapping effect of levels, tends to overestimate the value in Doppler broadening. On the other hand, "Method A," which is essentially a special case of "Method B" when ψ_K/β is much smaller than unity (which is the case for weak resonances) except for the overlapping and interference terms, also becomes questionable in the intermediate-energy region for the following reasons:

(1) The overlapping term $e(s)$, which depends on the spacing $\langle s \rangle$ and Doppler width Δ, no longer assumes the asymptotic value given by Nicholson when Γ_K/Δ becomes appreciable in the intermediate-energy region.

(2) The term $E(s)$ described by Nicholson is also dependent on the Doppler width Δ when Γ_K/Δ becomes appreciable.

(3) The contribution of the terms of higher order in the expansion become significant.

Theoretically, it is possible to extend the range of validity of "Method A" into a region of lower energy when these factors are taken into

---

[4]R. B. Nicholson, The Doppler Effect in Fast Neutron Reactors, APDA 139 (June 1960).

account. "Method A" when modified must approach "Method B" at some energy when the overlapping and interference terms become negligible.

An exact evaluation of the integral $\int_{-\infty}^{\infty} \psi_K \psi_{K'} \, dE$ has been carried out analytically by means of the Faltung theorem for Fourier transform. The result consists of Fresnel integrals $C(\delta^2/\langle s\rangle^2)$ and $S(\delta^2/\langle s\rangle^2)$.

The level-spacing-distribution function $\Omega(\delta)$ has been obtained for the case when $\nu = 8$. A code is now available to evaluate the integral $2\int_0^{\infty} \Omega(\delta)\, d\delta \int_{-\infty}^{\infty} \psi_K \psi_{K'} \, dE$. Some results of overlapping terms for U^{235} and Pu^{239} as compared to $\delta\tilde{\sigma}_x$ by "Method B" calculations are tabulated in Tables V and VI. The overlapping term "0" by which $\delta\tilde{\sigma}_x$ should be reduced becomes insignificant below 0.61 kev for U^{235} and 2.25 kev for Pu^{239}. The following set of parameters were used in the calculations:

(1) U^{235}:

$\langle \mu t/\rho \rangle$ = 200 barns per atom.

$\langle \Gamma f \rangle$ = assumed constant at 120 mv. s-wave only.

$\langle \Gamma_n^0 \rangle / \langle s \rangle = 1 \times 10^{-4}$.

$\langle s \rangle_3$ = 1.72 ev.

$\langle s \rangle_4$ = 1.34 ev.

ν = 1 for the neutron width frequency function.

η = 2 for the fission width frequency function.

(2) Pu^{239}:

$\langle \mu t/\rho \rangle$ = 200 barns per atom.

$\langle \Gamma_f \rangle$ = assumed constant at 99 mv.

$\langle \Gamma_n^0 \rangle / \langle s \rangle = 1 \times 10^{-4}$; s-wave only.

$\langle s \rangle_0$ = 11.58 ev.; $\langle s \rangle_1$ = 3.86 ev.

ν = 1; η = 2.

Table VI. "Method B" Calculations for Pu^{239}

	A: Changes in Pu^{239} Cross Sections (in barns) due to Changes in Doppler Broadening			B: Change in Reduction in Isolated-level Cross Sections in Pu^{239} due to Overlap (0)		
	Fission					
E(kev)	$\tilde{\sigma}_{f750°K}-\tilde{\sigma}_{f300°K}$	$\tilde{\sigma}_{f1500°K}-\tilde{\sigma}_{f300°K}$	$\tilde{\sigma}_{f2500°K}-\tilde{\sigma}_{f300°K}$	$\tilde{0}_{f750°K}-\tilde{0}_{f300°K}$	$\tilde{0}_{f1500°K}-\tilde{0}_{f300°K}$	$\tilde{0}_{f250}$ °K-$\tilde{0}_{f300°K}$
9.1	0.01395	0.02100	0.02480	0.001147	0.002262	0)03072
6.5	0.0190	0.0290	0.0350	0.001170	0.002560	0)03598
2.25	0.090	0.140	0.180	0.000566	0.00301	0)0617
	Capture					
E(kev)	$\tilde{\sigma}_{\gamma 750°K}-\tilde{\sigma}_{\gamma 300°K}$	$\tilde{\sigma}_{\gamma 1500°K}-\tilde{\sigma}_{\gamma 300°K}$	$\tilde{\sigma}_{\gamma 2500°K}-\tilde{\sigma}_{\gamma 300°K}$	$\tilde{0}_{\gamma 750°K}-\tilde{0}_{\gamma 300°K}$	$\tilde{0}_{\gamma 1500°K}-\tilde{0}_{\gamma 300°K}$	$\tilde{0}_{\gamma 250}$ °K-$\tilde{0}_{\gamma 300°K}$
9.1	0.00720	0.01101	0.01280	0.000657	0.001297	0)01727
6.5	0.0110	0.0170	0.0200	0.000882	0.001490	0)02075
2.25	0.050	0.080	0.100	0.000346	0.00185	0)0382

Table V. "Method B" Calculations for U^{235}

	A: Changes in U^{235} Cross Sections (in barns) due to Changes in Doppler Broadening			B: Change in Reduction in Isolated-level Cross Sections for U^{235} due to Overlap (0)		
	Fission					
E(kev)	$\tilde{\sigma}_{f750°K}-\tilde{\sigma}_{f300°K}$	$\tilde{\sigma}_{f1500°K}-\tilde{\sigma}_{f300°K}$	$\tilde{\sigma}_{f2500°K}-\tilde{\sigma}_{f300°K}$	$\tilde{0}_{f750°K}-\tilde{0}_{f300°K}$	$\tilde{0}_{f1500°K}-\tilde{0}_{f300°K}$	$\tilde{0}_{f250}$ °K-$\tilde{0}_{f300°K}$
12.05	0.0035	0.0053	0.0064	0.0009850	0.001525	(001840
6.5	0.00910	0.0140	0.0168	0.002480	0.003295	(003975
2.25	0.0428	0.0669	0.0808	0.008425	0.001525	(01940
0.61	0.2291	0.3718	0.4593	0.004145	0.01357	(04900
	Capture					
E(kev)	$\tilde{\sigma}_{\gamma 750°K}-\tilde{\sigma}_{\gamma 300°K}$	$\tilde{\sigma}_{\gamma 1500°K}-\tilde{\sigma}_{\gamma 300°K}$	$\tilde{\sigma}_{\gamma 2500°K}-\tilde{\sigma}_{\gamma 300°K}$	$\tilde{0}_{\gamma 750°K}-\tilde{0}_{\gamma 300°K}$	$\tilde{0}_{\gamma 1500°K}-\tilde{0}_{\gamma 300°K}$	$\tilde{0}_{\gamma 250}$ °K-$\tilde{0}_{\gamma 300°K}$
12.05	0.00157	0.00239	0.00284	0.000443	0.000705	(000832
6.5	0.00430	0.00650	0.00780	0.000995	0.001538	(001870
2.25	0.0220	0.0340	0.0408	0.00226	0.00757	(00118
0.61	0.1326	0.2110	0.2578	0.006566	0.01716	(02638

B. Reactor Fuels and Materials Development

1. Ceramic Fuels

a. Uranium-Plutonium-Carbide Fuel. Present work is directed toward (1) scale-up of PuC production to one-kilogram batches, (2) development of methods of filling jackets and of vibratory compaction that maintain the jacket weld exteriors free of contamination, (3) production of contamination-free welds, and (4) increasing the heating capabilities of furnaces until they can melt low-plutonium (U-Pu)C.

One-kilogram batches of plutonium and carbon were reacted and extensively sampled, analyzed, and examined metallographically to determine homogeneity.

Fixed alpha activity in the welds of jackets containing vibratory-compacted (Pu-U)C irradiation specimens has been a serious problem in the past. Procedures have now been developed which allow the jackets to be welded without contamination. This was accomplished by filling the jacket tube while it is in a protective Teflon sleeve. The fitting is sealed to the jacket by collodion. After the filling and compacting, the Teflon sleeve is taken off, and the collodion is removed by mechanical stripping and scrubbing with acetone and ether. Complete elimination of the collodion is the main problem. If any collodion residue remains, the result is a gassy weld.

Attempts to melt low-plutonium (U-Pu)C at temperatures above 2100°C resulted in the sagging and excessive carburizing of the innermost tantalum reflector in the melting furnace. A new reflector assembly has been designed for the carbon-resistance furnace. A graphite inner shield will be used to keep the first tantalum shield from "seeing" the graphite resistance coil. The number of reflectors has been increased to six, and a spun alumina liner has been installed in the furnace shell to reduce losses.

b. Uranium-Thorium Sulfide. The US-UOS system will be studied in some detail since the main secondary phase found in US is UOS. An initial attempt was made to synthesize UOS in a bomb in which a pelletized mixture of one part uranium powder, two parts sulfur powder, and one part UO_2 was reacted at 600°C for one hour in argon. The product contained estimated 80-90% UOS, the remainder being a mixture of UO_2, γUS_2, and U_2S_3. Apparently, the sulfur first reacted with the uranium to form US_2, and the heat from this reaction produced a sufficiently high temperature for most of the US_2 to react with the UO_2. Leaching with 10% H_2SO_4 improved the product only slightly.

A specimen for thermal-conductivity measurements was made by a paste-molding process. Uranium monosulfide was crushed in benzene to pass a 400 mesh sieve (37 μ). A 5% binder solution of stearic acid, acryloid, and carbon tetrachloride was added to form a heavy paste, which was charged gradually into an aluminum mold and vibrated until the paste became solid. The formed piece was dried and then sintered in vacuum at 1850°C for 2 hr.

The sintered specimen contained approximately 2.3 w/o of UOS, and had sintered to 97.0% of theoretical density. The material in the specimen had a slightly contracted lattice parameter of 5.4871 Å, which would indicate that some foreign anions were in solid solution.

Preliminary heat-conduction measurements over the temperature range from 100 to 400°C gave thermal conductivities of US as follows:

Temperature °C	Thermal Conductivity, cal/(cm)(°C)
100	0.0275*
200	0.0284
300	0.0298
400	0.0320

*These values are corrected to theoretical density.

Additional samples of uranium monosulfide have been prepared on a laboratory scale by the reaction of hydrogen sulfide with hydrided-dehydrided uranium metal, followed by homogenization at about 1900°C in vacuum. Recent preparations have shown no material that is insoluble in dilute sulfuric acid (a measure of oxygen-containing impurities). Sulfur-to-uranium ratios of these products range from 0.99 to 1.03.

c. Uranium, Thorium, Plutonium Phosphides. The objective of this study is to characterize the compounds in the various phosphide systems and to evaluate their potential as reactor fuel materials. Compounds are being synthesized by reaction of the solid elements and by reaction of uranium with phosphine gas.

Synthesis of uranium monophosphide by means of the phosphine reaction has been investigated in some detail. Reaction temperature has been varied in the range from 300 to 750°C. U_3P_4 was obtained at all temperatures, although small amounts of UP_2 occurred in material synthesized at 400°C. Reaction rates were relatively rapid at 300°C and 400°C, and condensation of white phosphorus was minimal at these temperatures. Reaction rates appeared somewhat slower at higher temperatures (500 - 750°C), and the deposition of phosphorus (this time admixed with red and black varieties) was extensive throughout the apparatus. Thus, it appears that the lower reaction temperatures are desirable from several standpoints. Calcination at 1400°C in vacuum of materials produced at the various temperatures resulted in a fairly high-purity UP (on the basis of X-ray diffraction). Chemical analysis will be conducted to verify this.

Decomposition of U_3P_4 into UP and P occurs below 1300°C in vacuum. Future experiments will bracket the decomposition temperature more closely. UP_2 decomposes very rapidly in vacuum at 700°C into U_3P_4 and P.

UP made by the phosphine reaction exhibited a melting point of about 2730°C. This melting temperature is about 100°C higher than that of material produced by the direct reaction of the elements. However, this is not surprising in view of the greater purity of the former material, which has about one-fifth the oxygen content of UP made from the elemental powders.

UP powder made by the phosphine reaction was fairly sinterable. Cold-pressed pellets sintered in vacuum at 2000°C had densities of about 90% of the theoretical value. Samples were sound and did not show the signs of surface crazing observed previously.

The lattice constant of UP has been observed to shrink with increased heating temperature. This is presumed to be a result of the irreversible loss of phosphorus at elevated temperature, producing a substoichiometric UP compound. Departure from stoichiometry increases at higher temperature, showing that the UP structure can tolerate a higher anion deficiency concomitant with the greater loss of phosphorus. The stoichiometric UP structure does not appear capable of accommodating excess phosphorus; below about 1300°C, U_3P_4 coexists with UP when the P/U mole ratio exceeds unity.

2. Corrosion Studies

a. Fuel-cladding Materials for Sodium-cooled Reactors. A sample of Nb-5 w/o Mo alloy exposed for 504 hr to flowing (2 ft/sec) sodium containing 1-5 ppm Na_2O at 650°C behave differently than other niobium-base alloys exposed in the same facility at the same time. A bend test showed no loss in room-temperature ductility. Oxygen content increased from an initial value of about 200 ppm to about 275 ppm after exposure. In contrast, a Nb-4.33 w/o Zr sample was completely embrittled and increased in oxygen content from 70 to 1100 ppm during the same test.

It is believed there may be a correlation between the behavior of refractory metals in oxygen-contaminated sodium and in oxygen at low pressure. If such a qualitative correlation does indeed exist, screening of candidate materials would be greatly facilitated. Accordingly, it is planned to study the oxidation behavior of likely materials in the temperature range from 500 to 700°C in argon containing about 10 ppm oxygen, prior to, or concurrent with, corrosion studies in sodium. Pending receipt of this gas mixture, tests are being run in pure oxygen (at about 1 atmosphere pressure) to obtain base-line data and to familiarize ourselves with the apparatus.

b. Structural Materials in Superheated Steam. A five-week exposure of Types 304 and 406 stainless steels has been completed in 650°C, 600-psig steam flowing at 100, 200, and 300 ft/sec. In these tests, the oxygen content was approximately 0.05 ppm as contrasted with the first experimental series operated at 30 ppm oxygen. As before, the samples were electropolished prior to exposure.

Corrosion results under the deoxygenated conditions were almost exactly the same as those obtained in oxygenated steam, an unexpected result. The corrosion rate of Type 304 was 3 to 4 mils/yr after the first two weeks, and pits, 3 mils deep, pocked the metal surface after removal of the corrosion coating.

As before, Type 406 stainless steel corroded about 0.1 mil independently of time of exposure or flow. This indicates a very low corrosion rate.

Currently, an oxygenated steam-flow test of four INCO alloys and GE René 41 alloy is being performed.

c. Zirconium Alloys for Superheated Steam. The exposure of zirconium alloys to oxygenated, 200-ft/sec flowing steam referred to in Progress Report for March 1963, ANL-6705, p. 43, is continuing. During the first two weeks of exposure the presence of oxygen had little, if any, effect on weight gains.

d. Miscellaneous Materials in Water and Steam. Rolled samples of "A" nickel on prolonged exposure to 650°C oxygenated steam began to gain weight rapidly and at 40 days had suffered extensive intergranular attack. Metallographic examination of the material in a swollen region showed intergranular corrosion throughout the area and a large void in the swollen material. The inner surface of the blister was covered with oxide.

This intergranular attack has not occurred in samples of rolled TD nickel. Metallographic examination showed a long, thin grain structure of sound metal, with a thin, nonhomogeneous corrosion film at the sample surface.

How the presence of 2% thoria as milli-micron particles distributed through the TD metal can impart this enhancement of corrosion resistance is not clear. Two approaches toward explaining this behavior have been suggested: (a) physical modification of the corrosion film because of the presence of thoria, and (b) electrical modification of the film properties at the test temperature, probably by an increase in conductivity due to thoria.

e. Corrosion Resistance of Urania Burnable Poisons. Urania-rare earth oxide compacts, sintered at 1700°C in hydrogen for 4 hr, were treated for 15 and 72 hr in 360°C oxygenated distilled water to complete the corrosion-resistance studies. (see Progress Report for March 1963, ANL-6705, p. 39). Weight losses occurred for all samples except the 3 w/o Gd_2O_3 - 97 w/o UO_2 sample after treatment for 15 hr. The weight loss in the 100 w/o UO_2 sample was appreciable. The gadolinia sample incurred an infinitesimal weight gain. A similar behavior was noted in the samples treated for 72 hr. The weight losses were greater than for the 15-hr treatment. Similarly, the gadolinia sample increased in weight as the exposure time increased.

Differential thermal analyses are being made on the mixtures of urania and rare earth oxides. No pronounced peaks have been established as characteristic of the rare earth oxides. Upon completion of the analyses

of the unsintered oxides, a study of hydrogen-sintered urania-rare earth oxide compositions will be made to establish solid solution limits.

f. Aluminum Powder Products. The French powder products are inspected every two months in a continuing aqueous corrosion test at 290°C. To date (after about 8 months) the samples are in very good condition.

Other samples of the same products are now being exposed to flowing water (18 ft/sec) at 315°C. The appearance after one month was very good. No blisters or other serious defects were noted.

3. Fuel-jacket Development for High-temperature Applications

A high-temperature, high-strength niobium alloy, D-43 (Nb-10 w/o W-1 Zr-0.1 w/o C), is being studied in addition to the two alloys (Ta-10 w/o W and Ta-18 w/o W-2 w/o Hf) previously mentioned in the Progress Report for February, ANL-6698, p. 41. All three alloys are now in the sizing and finishing stage for 0.156-in.-ID x 0.015-in. wall tubing.

4. Nondestructive Testing

a. Neutron Imaging. The neutron radiographic beam at the Juggernaut reactor has been studied to determine the influence of various graphite thicknesses in the beam tube. These studies were made without a collimator so that the emergent beam covered an area about $6\frac{3}{8}$ in. in diameter. At a reactor power of 200 kw, the total neutron flux at the reactor face varied from about 3×10^8 n/(cm^2)(sec) for no extra graphite in the beam tube to 2.5×10^6 n/(cm^2)(sec) for 30 in. of graphite. The cadmium ratio as determined by 0.020-in., cadmium-covered gold foils and bare gold foils varied from about 2 to greater than 4, and the gamma intensity varied from 650 r/hr to 70 r/hr over the same range of thickness of graphite.

A graphite thickness of 5 in., providing a total neutron flux of 3×10^8 n/(cm^2)(sec), a cadmium ratio of 2.1, and a gamma intensity of 480 r/hr, appears to provide a good compromise among the many factors involved in a beam choice. After collimation, this beam configuration promises to yield a neutron beam intensity several times higher than that used in our previous tests with a collimated beam. These beam studies are now being extended to include the collimated beam since, from a resolution point of view, this arrangement provides better imaging results than the large area beam.

b. Correlation of Heat-transfer Properties and Bond Quality. One of a series of ultrasonic tests using a through-transmission technique has been completed on copper-brazed specimens. These tests were run on different sensitivity levels of a "go-no-go" type of recording system. All specimens showed areas of nonbond or "weak" areas. Roll-bonded samples

of various composition whose histories are unknown were also tested. One of these has questionable areas and will be included in future studies.

At present, ultrasonic tests are being run with all these specimens and the recording system whose writing current is directly proportional to the signal output. Both through-transmission and pulse-echo methods will be used.

c. Application of Infrared Radiation to Nondestructive Testing. Investigation of the possible use of infrared in nondestructive testing has continued. An infrared imaging system that uses a spherical mirror to focus an infrared image on a screen of Radelin thermographic phosphor was investigated. The thermographic phosphor is excited by ultraviolet light. The brightness of the phosphor is temperature sensitive so that the infrared image becomes visible on the glowing phosphor screen. The infrared image of a hot plate with the letter M painted on it with flat black paint could readily be seen. This source was used to determine the effect of screen thickness on image sharpness. No attempt has been made to measure the temperature resolution.

The thermographic phosphor was also sprayed directly on the surface of test objects to reveal differences in surface temperature. Voids in a sodium-bonded test piece could be detected by the method. The technique of using thermographic phosphor to determine bond quality has been previously investigated and was found to be not sufficiently sensitive; however, the present phosphor is supposed to have improved temperature sensitivity.

A tuned amplifier is under construction for use with the indium antimonide detectors, and a larger spherical mirror has been obtained to improve the temperature resolution of this infrared-detecting system.

C. Heat Engineering

1. Studies of Boiling Liquid Metals

The program to develop and construct a liquid metal loop to perform experimental studies on heat transfer and fluid dynamics at high temperatures is progressing. Material and dimensional specifications have been prepared for columbium-1% zirconium piping, and firm estimates have been obtained for a large portion of the alloy. Design criteria for a vacuum containment system to protect the refractory metal from the atmosphere have been written, and requests for proposals have been submitted to various vendors. An overall cost estimate for the work has also been completed and a work project request initiated. Based upon the evaluation of funds, it is planned to proceed with the procurement of the vacuum equipment but defer final design and fabrication of the columbium-alloy loop and concentrate upon development of heating sections,

instrumentation, operational methods, and fabrication techniques with a stainless steel loop designed for lower temperatures.

Drawings have been completed for a boiling liquid metal heat transfer loop constructed of Type 316 stainless steel. Both electron- and radiant-heated sections are to be used. The electron-heated section will be used to study heat transfer coefficients of liquid metals flowing in an annular section, while the radiant-heated section will be used to study heat transfer of a liquid metal flowing in a tube. The electron-heated section has been described in Monthly Progress Report for September 1962, ANL-6619, p. 45.

The radiant-heated section consists of a thick-walled molybdenum-0.5% titanium tube surrounded by a cylindrical tungsten heater. Thermocouples will be placed at various radial positions inside the tube wall so that wall temperatures can be measured.

2. Stability and Pressure Control in Boiling-Condensing Flow Systems

After minor modifications, the Armadilla boiling-condensing flow loop was operated as a closed recirculating system with forced and natural circulation to investigate pressure control and stability. When the generated steam was condensed in the throttled inlet-exit section paralleling the main recirculating flow stream, the pressure stability was excellent with both forced and natural circulation. The inherently low available pressure difference across the steam-condensing section, however, prevented an adequate steam flow, and the system pressure could be controlled only over limited power ranges. Adequate pressure control was achieved by throttling the inlet steam or regulating the coolant water by bleeding either generated steam or recirculating water from the system, although this practice does not meet the fully closed system criteria.

Assuming the availability of an adequate pressure difference across a similarly throttled condensing section, it appears that a fully closed boiling-condensing liquid metal system could be operated stably and with acceptable control of the system pressure.

3. Heat Transfer in Double-pipe Heat Exchangers

Sufficient progress has been made in the analytical study of heat transfer between fluids of low Prandtl number in double-pipe heat exchangers (see Monthly Report for February 1963, ANL-6698, p. 43) to warrant publication. A paper is being prepared that will describe the analysis and results for cocurrent flow cases. These studies serve as a means for determining liquid-metal heat transfer coefficients.

Since the last progress report, two important additions to the previous analyses have been completed: (1) extension of the plug flow solutions

to the case of a double-pipe heat exchanger configuration consisting of a circular tube surrounded by a thin annular space; and (2) the discovery of a relatively simple approximation technique to solve slug flow cases for turbulent flow having Peclèt numbers of at least 1000.

The analyses have yielded a variety of interesting results, some of which may appear to be contrary to expectation. Although these will be described in detail in the paper now being written, several points deserve brief mention here.

(1) Values of fully developed heat transfer coefficients in cocurrent-flow double-pipe heat exchangers can be significantly lower than those corresponding to the boundary condition of uniform wall temperature, but never larger than those corresponding to the boundary condition of uniform wall heat flux.

(2) Under certain operating conditions, local heat transfer coefficients in cocurrent-flow, double-pipe heat exchangers do not decrease monotonically with distance from the exchanger inlet, but, instead, attain a minimum value and then increase towards a fully developed (asymptotic) value.

(3) When operating a cocurrent-flow double-pipe heat exchanger with constant mass flow rate (or Peclèt number) through one channel, while varying mass flow rate (or Peclèt number) through the adjacent channel, the measured dependence of the fully developed heat transfer coefficient (or Nusselt number) on Peclèt number will be less than for the case of uniform wall temperature or uniform wall flux. Under certain operating conditions, the heat transfer coefficient will <u>decrease</u> with increasing Peclèt number.

This last observation is illustrated in Figure 16 in which computed values of Nusselt numbers vs. Peclèt numbers for the turbulent flow of a liquid metal are graphed. Values of Nusselt numbers for one side of a parallel-plane, double-pipe heat exchanger are plotted with constant Peclèt numbers of the fluid in the adjacent channel as a parameter. The Nusselt number vs. Peclèt number relationships for uniform wall temperature and for exchanger operation with Peclèt numbers equal on both sides, are also shown.

4. Boiling Simulation Loop

The correlation of void fraction and void profile data for two-phase water flow through the porous tube which was simulated with gas injection in water was completed. A phenomenological model for void profiles in this system is being developed.

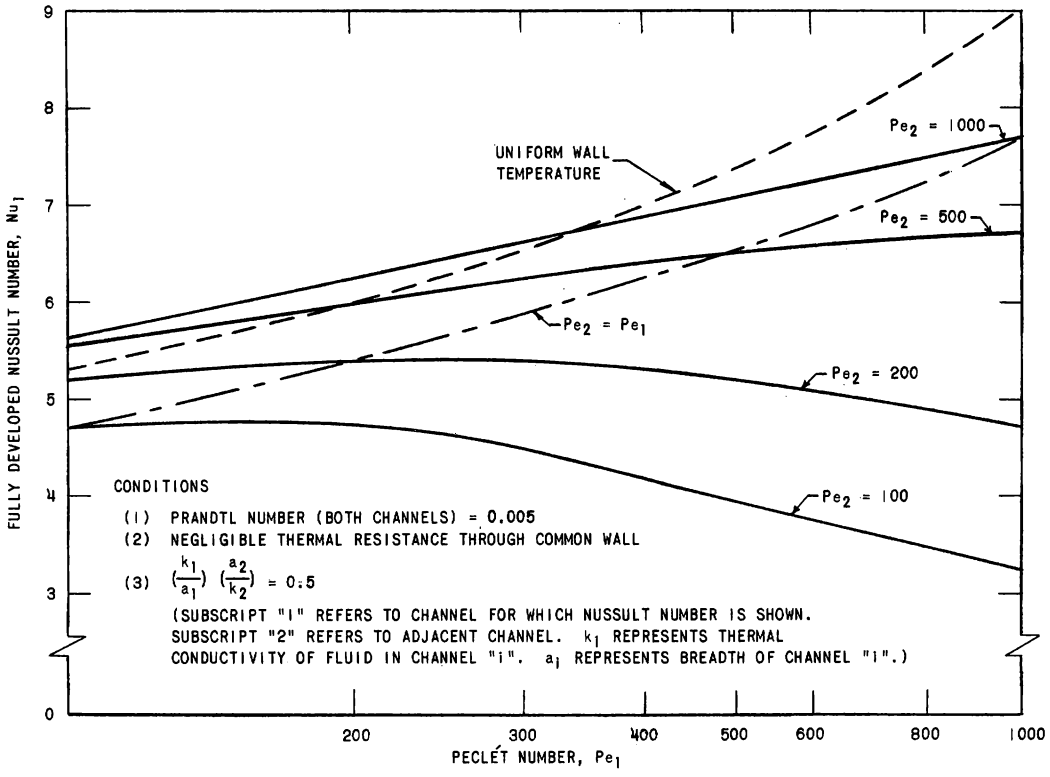

Figure 16. Fully Developed Nusselt Numbers for Cocurrent Turbulent Flow in Adjacent Parallel-Plane Channels as a Function of Peclèt Numbers in Both Channels.

The boiling simulation loop instrumentation and construction for running with heat addition were completed. Preliminary runs to check the system have been started.

5. Two-phase Critical Flow and Associated Problems

The flow of steam-water mixtures from various apertures in a high-pressure vessel containing saturated or slightly subcooled liquid is being investigated. The studies are related to the problem of containment when a reactor pressure vessel fails. All equipment and instruments have now been installed. Preliminary runs have indicated that methods planned for measuring transient flow rates, temperatures, and pressure gradients are satisfactory.

At present, data with a $\frac{1}{4}$-in. orifice are being obtained. The reduction of these data is in progress.

6. Mercury Condensation

This study will investigate the large differences which exist between theory and practice in the performance of some liquid metal condensers.

A rotating disk-type experimental condenser has been built. The apparatus has a 3-in.-diameter rotating disk condenser and will be used with mercury vapor. Thermocouples have been installed in the disk-rotating shaft assembly. The shaft has been dynamically balanced and installed in the condenser vessel. After the electromagnetic condensate flowmeter is calibrated in the loop and the slip-ring thermocouple assembly is completed, cold (noncondensing) runs will be made at several speeds up to 2500 rpm to check out the mechanical performance of the slip rings, rotary-seal, and mercury-lubricated Stellite sleeve bearing. The cold runs will be followed by condensing runs. The speed of the disk determines the thickness of the condensate film on the disk.

A Tm^{170} source of gamma radiation will be used to measure condensate film thickness. Attenuation measurements using gold foils have been made. The accuracy appears to be about 10 to 15% for films around 0.3 mil thick. The accuracy for films around 5 to 10 mils thick has not been determined, but the accuracy is expected to decrease with increasing film thickness due to complications introduced by the critical absorption of the 84-kev gamma ray and subsequent fluorescence. Improving the accuracy of this method for films up to 10 mils in thickness is under study.

D. Chemical Separations

1. Chemical-Metallurgical Process Studies

a. Chemistry of Liquid Metals. The thermodynamics of the plutonium-cadmium system is being studied by the galvanic cell method. Preliminary emf data for the cell

$$Pu/PuCl_3, LiCl\text{-}KCl \text{ (eutectic)}/Pu\text{-}Cd \text{ (2-phase alloy)} \quad ,$$

have been obtained over the temperature range from 350 to 612°C. A peritectic transformation at 403°C is indicated. This is in excellent agreement with the results of solubility studies of plutonium in cadmium, which place the peritectic transformation at 404°C. The latter data have been fitted to the equations:

$$(330 \text{ to } 404°C) \text{ Plutonium: } \log(\text{atom percent}) = 5.7916 - 4040.6\ T^{-1} \quad ;$$

$$(404 \text{ to } 505°C) \text{ Plutonium: } \log(\text{atom percent}) = 3.2293 - 2304.8\ T^{-1} \quad .$$

b. Reduction of Thorium Dioxide. Further experiments have been performed on the reduction of thorium dioxide by liquid magnesium-zinc alloy in the presence of molten 10 mole percent magnesium chloride-magnesium fluoride flux at about 800°C (see Progress Report for January 1963, ANL-6683, p. 40).

c. Uranium Oxide Reactions in Molten Halides. Further investigations have been carried out on the thermal decomposition of uranyl chloride

at 650°C in molten chloride media (see Progress Report for March 1963, ANL-6705, p. 49). Preliminary measurements of the equilibrium constant

$$K = \frac{\left[UO_2Cl\right]^2 \left[P_{Cl_2}\ (atm)\right]}{\left[UO_2Cl_2\right]^2}$$

at 650°C have given values of 1×10^{-3} atm in the ternary eutectic, lithium chloride-sodium chloride-magnesium chloride, and about 2.7×10^{-3} atm in the binary eutectic, lithium chloride-potassium chloride.

2. Fluidization and Volatility Separations Processes

a. Fluoride Separations. Additional data have been obtained for the alpha-induced decomposition of gaseous plutonium hexafluoride to plutonium tetrafluoride and fluorine, either alone or in the presence of nitrogen, helium, or krypton (see Progress Report for January 1963, ANL-6683, p. 41). The decomposition rates for 50, 71, 98 and 100 mm Hg samples of plutonium hexafluoride at about 25°C were determined in runs which varied in duration from 229 to 386 days. The runs were carried out in nickel spheres having volumes of about 125 cc. The results of these runs, which are summarized in Table VII show the following effects on the average decomposition rate of plutonium hexafluoride: (1) a decrease with increasing storage time, (2) a significant decrease upon addition of fluorine, (3) a slight decrease upon the addition of krypton, and (4) no significant effect upon the addition of helium. In runs with nitrogen as the additive, nitrogen trifluoride (NF_3) was found. The mechanism by which the nitrogen trifluoride was formed is not yet known. About 79, 92, and 97 percent of the plutonium hexafluoride (initially present at 100 mm Hg pressure) decomposed after 230 days in mixtures containing 2.7, 0.8, and 0.8 atm nitrogen, respectively, as the additive.

Evaluation of high-efficiency filters, which are employed in the ventilation systems of facilities used for handling plutonium hexafluoride, was continued (see Progress Report for January 1963, ANL-6683, p. 41). The efficiency of the filters in removing plutonium hexafluoride from air streams by combined vapor-phase hydrolysis and filtration is being determined. In current experiments, which were carried out with dilute uranium hexafluoride in laminar-flow equipment, two dilute streams of the reactants were allowed to mix by diffusion while flowing through the equipment. The uranium hexafluoride pressures ranged from 0.0051 to 0.059 mm Hg in the one stream, and the water vapor pressures ranged from 0.79 to 7.6 mm Hg in the other stream. In both streams, nitrogen was the carrier gas. The resulting mixed stream was filtered by a stack of four filter discs (absolute-type filter media). Results of the filtration of the hydrolysis products indicate that the kinetics of the hydrolysis reaction affect the filtration. For uranium hexafluoride pressure of 0.005 mm, water vapor pressure of 0.8 mm, and hydrolysis reaction time of 13.5 sec,

the penetration of the first filter was 14 percent. Increase of the water vapor pressure to 8 mm decreased the penetration of the first filter to 0.8 percent. If diffusion between the two reactant streams were the rate-determining factor, the reaction would be complete with less than 0.07 mm of water vapor.

Table VII. Alpha-Induced Decomposition of Plutonium Hexafluoride

Sample Storage Vessels: Nickel spheres of 125 to 128 cc volume
Storage Temperature : 26 ± 2°C

Decomposition Time (days)	PuF_6 (mm Hg)	Second Gas Component		Average Rate of Decomposition (%/day)
		Gas	Pressure (mm Hg)	
229	50	None	0	0.16
232	50	None	0	0.19
386	71	None	0	0.13
327	98	None	0	0.091
327	98	None	0	0.083
229	100	None	0	0.16
386	100	None	0	0.076
229[a]	100	Fluorine	2,280	0.026
231[a]	100	Fluorine	682	0.029
229[a]	100	Krypton	3,720	0.11
231[a]	100	Krypton	695	0.073
231[a]	100	Krypton	673	0.081
229[a]	100	Helium	2,230	0.11
231[a]	100	Helium	680	0.14
231[a]	100	Helium	677	0.12

[a]The second gas component was added 11 days after the experiment was started.

The absorption spectra of gaseous plutonium hexafluoride and uranium hexafluoride were determined in the visible and near infrared regions. Previously reported results indicated the possibility of utilizing the difference in absorbancies of plutonium hexafluoride and uranium hexafluoride in the ultraviolet region for inline process analysis by absorption spectrophotometry (see Progress Report for December 1962, ANL-6672, p. 35). At 3400 Å, the ratio of molar extinction coefficients of gaseous plutonium hexafluoride to uranium hexafluoride is approximately 600.

The absorption spectra of gaseous plutonium hexafluoride and uranium hexafluoride were obtained in 5- and 10-cm-long nickel cells

having quartz windows at gaseous sample pressures which ranged from 11.5 to 105 mm Hg pressure.

The spectrum of gaseous uranium hexafluoride in the visible and near infrared regions shows very little if any absorption at pressures up to 105 mm in a 5-cm-long cell. In the ultraviolet region, however, uranium hexafluoride is a strong absorber. The spectrum of plutonium hexafluoride also shows a number of peaks in the visible region, several bands with fine structure between 7,800 Å and 11,000 Å and several minor peaks remaining in the near infrared region. Like uranium hexafluoride, plutonium hexafluoride absorbs strongly in the ultraviolet.

Plutonium hexafluoride and possibly uranium hexafluoride slowly etch the quartz glass windows. To compensate for the change in the transmittancy of the windows, a large correction is required in the ultraviolet region. The correction required increases with time of exposure of the quartz glass to the hexafluoride mixture. Since no corrections are needed at longer wavelengths, inline process analysis using the near infrared region for the absorption measurements is being considered.

b. Direct Fluorination of Uranium Dioxide Fuel. The development of a two-zone oxidation-fluorination scheme for the conversion of uranium dioxide pellets into uranium hexafluoride in a single reactor was continued in engineering-scale studies (see Progress Report for February 1963, ANL-6698, p. 48). In this scheme, there are two distinct reaction zones. The first is a bed of uranium dioxide pellets with alumina particles in the voids of the bed; the second is a bed of alumina particles placed over the uranium dioxide pellet bed. In the pellet-bed zone, U_3O_8 fines are produced by contacting the uranium dioxide with an oxygen-nitrogen stream which also serves to fluidize the alumina particles. The U_3O_8 fines are elutriated from the lower zone and are reacted in the upper zone with fluorine, which is admitted to the fluidized bed of alumina just above the uranium dioxide pellet bed. The fluidized alumina not only serves as a heat transfer medium, but also appears to aid in the transport of the U_3O_8 fines to the fluorination zone.

In two previously reported runs (see ANL-6698, p. 48), 12-in.-deep static beds of uranium dioxide pellets (8.8 kg) were processed in 15 hr with 4.5 percent oxygen in nitrogen and in 12.5 hr with 6 percent oxygen in nitrogen. Overall fluorine efficiencies for these runs were about 70 percent. In these runs, the temperature of the upper zone was maintained at 500°C and no attempt was made to maintain predetermined temperatures in the pellet bed. Fluorine input to the fluorination zone was diluted by a partial recycle of off-gas (0.25 scfm) to prevent plugging of the fluorine inlet. Gas pulsing was used to aid in fines transport from the oxidation to the fluorination zone.

Another run has been completed in this series in which the effects of gas pulsing and low concentrations of oxygen in the oxidation zone were studied further. In this run a 12-in.-deep static pellet bed was again used. The temperature in the fluorination zone was maintained at 500°C as in the previous runs, and again no attempt was made to keep the temperature of the pellet zone at a predetermined temperature. In the oxidation zone, the composition of the fluidizing gas was 8 percent oxygen in nitrogen with a gas flow of one scfm. The gas flow in the fluorination zone was 1.5 scfm and the concentration of fluorine in the gas mixture was from 9 to 15 percent. A small amount of gas (about 2 percent of the total gas flow) was added in pulses at a frequency of 2 pulses per minute and a pulse duration 0.04 sec. The uranium dioxide charge was completely fluorinated in a total processing time of 12.5 hr and with an overall fluorine efficiency of about 75 percent. The total processing time included a period (3.25 hr) of alumina bed cleanup with fluorine. Ninety percent of the product was collected in the first 8.2 hr of fluorination, corresponding to a production rate of 54 lb UF_6/(hr)(sq ft) and a fluorine efficiency of 79 percent.

It is believed that operating conditions in the run are closer to the optimum than in previous two runs. Improved control of the reaction was evidenced by more uniform rates of production of uranium hexafluoride and by higher fluorine efficiency for the complete batch operation. The continuous monitoring of fluorine in the process off-gas with a newly installed gas thermal conductivity cell assisted in the improved process control.

c. Decladding of Fuel Elements by Fluid-bed Oxidation. The development of a fluid-bed oxidation method for the separation of uranium dioxide pellets from stainless steel cladding in typical fuel elements is continuing (see Progress Report for March 1963, ANL-6705, p. 50). In this method, the uranium dioxide is oxidized with air to a higher oxide (U_3O_8). The uranium dioxide pellets break into fragments because of the large internal stresses produced by the difference in densities of the two oxides (UO_2 and U_3O_8). The U_3O_8 fines produced in the oxidation zone of the two-zone oxidation-fluorination reactor are elutriated to the fluid-bed fluorination zone.

Four additional engineering-scale runs have been made in which about 1-in.-long simulated fuel elements (stainless steel-clad uranium dioxide pellets) were oxidized with air at a superficial gas velocity of about 0.75 ft/sec. The wall thickness of the cladding in these runs was 0.010 in. instead of the 0.035 in. previously used. The $\frac{1}{2}$-in.diameter tubing elements were charged to the 2-in.-diameter fluid bed as random-packed beds of 40 elements. The results of these runs indicated the following (1) Gas pulsing (with air) was only partially beneficial for improving the rate of removal of oxide and for improving temperature uniformity in the system. Pulses of 1-sec duration were used at two frequencies, 0.5 pulse/min and 6 pulse/min, and in most runs the fluidizing gas

was cut off during pulsing to enhance the pulse effect. Variations in pulse techniques had little effect on the amount of uranium dioxide removed (60 to 70 percent). (2) An optimum overall rate of uranium dioxide removal appeared to occur at temperatures between 400 and 500°C.

Two successive steps are involved in the removal of uranium dioxide from the cladding: the chemical oxidation and the physical removal. The progress of the chemical step was followed independently by the determination of oxygen consumption with a gas thermal conductivity cell calibrated for oxygen-nitrogen mixtures. It was found that the oxidation was complete in 7 hr at 550°C and in 9 hr at 450°C. These results indicate that it is unlikely that the remaining residues can be separated by extending the operating time.

Difficulty in obtaining complete physical removal was encountered in all tests made thus far. Reasonable rates of removal were obtained up to 80 percent removal, but overall removals of greater than 80 percent were not obtained. Somewhat higher removals were obtained in tubing elements located at the top of the bed than at the bottom.

Other chemical treatments are being considered for the removal of caked oxide residue inside the tubing elements. Two possible methods are (1) a reduction with hydrogen, followed by re-oxidation, and (2) fluorination.

A mechanical method of breaching the stainless steel cladding (see Progress Report for February 1963, ANL-6698, p. 50) is also being evaluated as an aid to the oxidation of the uranium dioxide pellets. The method that is currently being considered involves the grinding of a line of holes along the longitudinal axis of the cylindrical cladding. It has been demonstrated that such a line of holes can lead to the rupture of the cladding during the oxidation process, and that complete oxidation of the pellets can thereby be attained.

d. Separation of Uranium from Zirconium Alloy Fuels. The development of a chlorination-fluorination scheme for reprocessing highly enriched uranium-zirconium fuels was continued. In the present scheme, the fuel is first reacted with hydrogen chloride in a fluidized bed of inert solids. This reaction converts the zirconium to the tetrachloride and the uranium to the trichloride. Since the hydrochlorination step is carried out at temperatures above the sublimation point of zirconium tetrachloride (331°C at 1 atm), a separation of the zirconium tetrachloride from the solid uranium trichloride is achieved. The uranium trichloride is then converted to the volatile uranium hexafluoride by reaction with fluorine and is thereby removed from the inert solids of the fluidized bed.

An additional run with miniature, multiplate alloy fuel subassemblies (see Progress Report for March 1963, ANL-6705, p. 51) was

carried out. Each subassembly weighed about 180 g and contained 2 g of uranium. The objectives of this experiment were the following: (1) evaluation of the less expensive Type 38 Alundum for use as an inert fluid-bed solid instead of Type RR Alundum which had been used in previous experiments, and (2) evaluation of the effect of re-using Type 38 Alundum in the off-gas filter on the buildup of uranium in the filter.

The run cycle included a hydrochlorination period of 8.3 hr for the first subassembly and a period of 5.3 hr for the second subassembly. The alloy temperatures of the subassemblies during the hydrochlorinations ranged from 345 to 575°C for the first subassembly and from 355 to 750°C for the second. The fluorination consisted of a one-hour fluorination period at 250°C followed by a 2-hr period at 500°C.

A residual uranium content of 0.01 w/o was retained by the Type 38 Alundum (320 g) in the fluid bed. This value is the same as that obtained in a previous experiment in which the fluorination time at 500°C was one hour and in which 320 g of Type RR Alundum was used (see ANL-6705, p. 52). Thus, it appears that equally good removals of uranium can be achieved with the two types of Alundum but, in order to achieve this end, a longer fluorination period is required with Type 38 Alundum. No buildup of uranium was noted in the off-gas filter when Type 38 Alundum was re-used (for a total of three subassemblies); the residual uranium content of the filter bed remained constant at 0.007 w/o.

IV. PLUTONIUM RECYCLE PROGRAM

New multigroup cross sections have been derived for use in calculating the initial core loading and first burnup step in the plutonium recycle loading of the EBWR. These cross sections were obtained through use of the Pu^{240} resonance parameters recently inserted into the GAM-1 code and of a free hydrogen gas model in the SOFOCATE code for the thermal group. Thermal disadvantage factors appropriate to the 2.5 percent enriched plutonium region are also included in the new cross sections, and an allowance of 0.03 has been included for effects of equilibrium xenon and samarium reactivity.

Recent hydrodynamic calculations indicate that the average core void fraction at 60 Mw is about 0.28. This value is considerably higher than original estimates of the void fraction which were used in the original survey calculations. Calculations indicate that for the 2.5 percent plutonium loading and 6 percent U^{235} shim containing europium and samarium at about 12 and 20 gm per element, respectively, the system is critical with an average core void fraction of about 0.22. This implies that the system will be operated at a power of less than 50 Mw instead of the earlier predicted 60 Mw. A new set of hydrodynamic calculations will be made to correlate more accurately regional power and voids at an output of 40 Mw.

Physics calculations are currently being made to establish the soluble poison (boric acid)requirements for reactivity control.

The new computer code, CHOPPED, (see Progress Report for February 1963, ANL-6698, p. 53) is not yet in operation, but should be available in time to simplify the described iterative procedures at other reactor power levels.

V. ADVANCED SYSTEMS RESEARCH AND DEVELOPMENT

A. Direct Conversion Studies

The behavior and general characteristics of the cesium-diode cell were further investigated.

The ionization of the cesium vapor was measured by applying a negative voltage to the collector and grounding the emitter.

The cesium vapor pressure was maintained as constant as possible during the experiments. While the emitter temperature was kept at a certain value, the voltages applied to the collector were varied from -5 to -200 v. Subsequently, the emitter temperature was increased and the voltage variations repeated. As the applied voltage was varied, it was found that the ion currents remained constant over the voltage range from -5 to -10 v, increased at higher voltages, but returned after some few minutes to the values found at -10 v or lower.

At higher emitter temperatures, the ion currents increased rapidly at first, but seemed to approach a limit at an emitter temperature of 2700°K and a cesium vapor pressure of 3-8 x 10^{-4} mm Hg (a density of 3 x 10^{12} to 10^{13} atoms/cc). The results indicate that a sheath screens the ion-producing emitter very effectively against an applied voltage, except for an initial shock that produces an ion-current surge. Increasing emitter temperatures produced more electrons in the sheath region that tended to reduce the positive space charge and permitted higher ion currents to flow from the emitter to the collector.

Theoretical calculations were made to estimate the saturation ion current expected for a given cesium concentration. It was found that the experimental values were two or three times higher than the calculated values.

B. Magnetohydrodynamic Power Generation

A meter is required for use in the magnetohydrodynamic (MHD) system for measuring flow rate of liquid metals at high temperatures and velocity without introducing perturbations in the stream. A flow meter, based upon the rate of heat loss to the passing liquid is being investigated for this application. This device consists of a copper sleeve in which a heater element and a thermocouple are embedded in close proximity. Power is supplied by a battery and monitored with conventional instruments. A temperature-compensated thermocouple is also located upstream in the flow. These two couples are differentially connected to eliminate any contribution of temperature of the ambient fluid. On the other hand, the heater

temperature for a fixed power setting is recorded as an excess voltage by the embedded thermocouple. This signal is an inverse function of the flow rate.

This model was constructed and the results of the trial operations were promising.

A family of calibration curves is now being constructed, since the flowmeter reading is sensitive to the ambient fluid being measured. The flow rate is determined by recording the output of the embedded thermocouple and reading the flow rate from the proper curve.

VI. NUCLEAR SAFETY

A. Thermal Reactor Safety Studies

1. Metal Oxidation and Ignition Studies

Studies of the oxidation of uranium by air were continued (see Progress Report for March 1963, ANL-6705, p. 63). The apparatus used consists of a convection-flow loop in which the sample, a one-cm cube of uranium, is mounted on a thermocouple in the lower part of the hot leg of the loop. This portion of the loop is heated (roughly to about 200°C) by a resistance heater located above the uranium sample. The leg on the opposite side of the loop is water cooled. The sample is heated by an induction heater. The apparatus is constructed of copper except for a glass section surrounding the sample. A schematic diagram of the apparatus is shown in Figure 17.

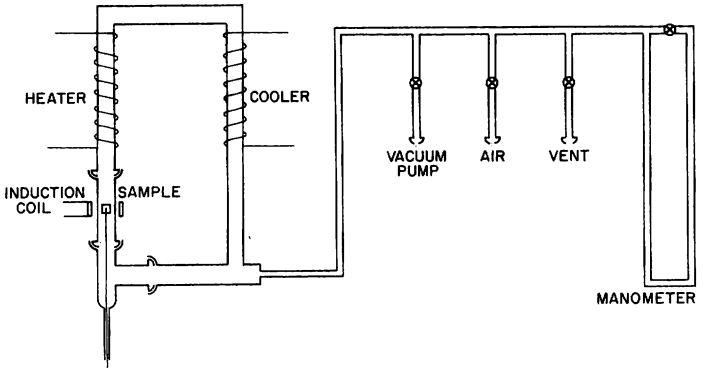

Figure 17

Schematic Diagram of Apparatus Used to Determine Uranium-Air Oxidation Kinetics

The oxidations were conducted by circulating air cooled to room temperature over the uranium cubes which were heated to 600°C and above. A recording pressure transducer was used to follow the decrease in the total pressure in the closed loop. Data from blank runs with a platinum sample were used to correct the observed pressure changes resulting from the heating of the specimens. The results of blank runs indicated that no loss of oxygen by reaction with the copper tubing used in the construction of the loop occurred after the first few runs. Preliminary results have indicated that a para-linear reaction (initially a parabolic rate followed by a linear rate) occurred over the temperature range from 600 to 800°C. A parabolic rate law was followed at 900 and 1000°C. Additional experiments will be carried out to verify these results. Experiments in which pure oxygen will be used are also being planned.

Burning-curve and shielded-ignition experiments with plutonium foils were performed in air and oxygen. In the burning-curve experiments the sample is heated at a uniform rate (usually 10 deg/min) in a flowing

atmosphere of the oxidant. As the rate of reaction increases, the sample self-heats and finally ignites. The temperature at which the sample ignites is determined by a graphical method. In the shielded-ignition experiments, the sample is first brought to test temperature in a protected atmosphere (usually helium) which is then rapidly replaced by the oxidant to determine whether ignition will occur at the test temperature.

Plutonium foils having thicknesses of 1, 0.5, 0.22, 0.17, and 0.12 mm were used in the experiments to obtain information on the relationship between the ignition temperature and the specific area of the foil. All foils used were about 3 mm wide and 20 mm long. The results of the experiments are given in Table VIII.

Table VIII. Ignition Temperatures of Plutonium Foils in Air and Oxygen

Foil Thickness (mm)	Specific Area (sq cm/g)	Burning-curve Ignition Temperature (°C)		Shielded-ignition Temperature[a] (°C)	
		Air	Oxygen	Air	Oxygen
1.0	1.5	322	490	378-408	327-374
0.52	2.5	310 314	468	303-337	353-398
0.22	5.3	518 520 535 519[b] 521[b]	524 527	375-403	322-350
0.17	6.7	282	299		
0.12	11.0	282	305	266-280	273-284

[a]Indicated as the lowest temperature at which ignition occurred and the highest temperature at which ignition did not occur. The shielding atmosphere was helium.

[b]Samples were polished with 600 grit silicon carbide paper; all other samples were as received.

The ignition temperatures ranged from 520 to 280°C with increasing specific area; however, a discontinuity in the ignition temperatures occurred at a specific area of about 5 sq cm/g (0.22-mm-thick foil). It is possible that the discontinuity may be associated with the change in kinetics between 320 and 420°C which was observed in the isothermal experiments previously reported (see Progress Report for March 1963, ANL-6705, p. 63).

2. Metal-Water Studies

Studies of isothermal uranium-steam reactions were continued in the modified apparatus which was previously described (see Progress Report for March 1963, ANL-6705, p. 64). In these experiments, uranium discs, $\frac{7}{8}$ in. in diameter and $\frac{1}{2}$ in. thick, are supported on a quartz pedestal and are heated by induction in flowing steam. This method of sample support was effective in preventing sagging and cracking of the oxide film at temperatures well above the melting point of uranium. The temperature of the metal was determined by placing a platinum, platinum-rhodium thermocouple in a hole at the center of the specimen. Temperatures determined at the outer oxide surface by an optical method were several hundred degrees lower than the metal temperatures. This difference in temperatures results from the insulating character of the oxide coating. The extent of the oxidation was followed by continuous volumetric measurements of the hydrogen that was evolved in the reaction.

In the present experiments, the temperature range over which the isothermal oxidations were studied was extended from 1200 to 1600°C. The parabolic rate law which was found in previous studies to apply to oxidations carried out at temperatures from 600 to 1200°C was found to apply equally well to reactions carried out between 1200 and 1600°C.

Three in-pile experiments in TREAT were completed with one aluminum-clad and two unclad aluminum-uranium alloy fuel plates. The transient energies were high and imparted 855 cal/g in the case of the aluminum-clad sample, and 880 and 1380 cal/g in the cases of the unclad fuel plates. It is likely that the temperatures of the plates greatly exceeded 1800°C, the temperature at which the vapor-phase burning of aluminum begins. The extent of reaction in the three experiments was 20, 27.4, and 43.2 percent for energy inputs of 855, 880, and 1380 cal/g, respectively. The average particle sizes of the residues were 83, 61, and 12 mils, respectively. Four additional experiments were carried out with uranium-aluminum fuel specimens in water heated to 280°C (vapor pressure of 1000 psi) in order to determine the effect of increased water temperature and pressure. The results of these experiments are not yet available.

Heating of a small metal particle to a high temperature while the particle is submerged in water will be attempted in a new series of experiments. The heating source will be an intense light beam from a ruby laser. It is hoped that the metal-water reaction of single spheres and discs with diameters from 0.3 to 1.5 mm can be studied by this method. In preparation for these studies, spheres of zirconium, uranium, and stainless steel are being prepared by rapidly melting wires of these metals in an inert atmosphere by imparting energy to the wires from discharging condensers. Aluminum spheres of suitable size will be purchased or prepared by etching larger specimens. Samples in the form of discs are available as punchings from foils.

The energy from the laser beam, 30 joules or 7 cal, is sufficient to heat the metal particles to very high temperatures (of the order of 3000°C) in less than one millisecond. The extent of reaction will be measured by micro-analysis of the hydrogen generated in the metal-water reaction and by metallographic determination of oxide film thickness. A photoelectric pyrometer will be constructed for the determination of the peak temperatures reached by the particles.

B. Fast Reactor Safety Studies

Fast power reactors are characteristically designed to contain sufficient fuel to produce a superprompt critical assembly if the core were rearranged into a sufficiently compact mass. Hence, it is possible to postulate a class of "meltdown" incidents in which the core is subjected to abnormal operating conditions, some degree of fuel failure occurs, and the fuel moves into a more compact mass that results in a destructive burst of nuclear power. It is of interest to understand the detailed mechanisms involved in the rearrangements of fuel and, if possible, to develop designs which will eliminate the possibility of violent disassociation.

TREAT is being used to perform in-pile experiments to study the characteristics of failure in fast reactor fuel elements, and to survey the mechanisms influencing movement of fuel.

1. In-pile Failure Times for Type 304 Stainless Steel-clad Uranium Fuel Pins

Experiments are being performed in TREAT to measure the failure times for penetration of EBR-II Type 304 stainless steel tubing by uranium or uranium-5 w/o fissium fuel pins. Tests on failure of uranium-5 w/o fissium pins were reported previously (see Progress Report for February 1963, ANL-6698, p. 65; and Progress Report for March 1963, ANL-6705, p. 16). Maximum clad temperatures were in the approximate range from 1130°C to 1200°C for the uranium samples. Failures occurred for six sodium-bonded pins for "time at temperature" ranging from 0.8 to 1.2 sec. Results from four unbonded specimens were erratic, and failure times (of 1.3 and 1.5 sec) could be obtained for only two of them. Although the failure times under irradiation do not show the same detailed temperature dependence obtained from penetration tests performed in isothermal furnace dip experiments, such failure times are in agreement with the furnace tests averaged over the approximate temperature range from 1130 to 1200°C.

2. In-pile Tests of Sintered Uranium Sulfide Pellets

Five exposed half-length EBR-II-sized, tantalum-clad uranium sulfide fuel samples (see Progress Report for March 1963, ANL-6705, p. 64) have

been examined. The general appearance of the sulfide pellets was good (see Table IX and Figures 18 and 19). No evidence was found for either a central cylindrical zone of granular appearance (found in uranium oxide samples of the same size which attained cladding temperatures above 1600°C as a result of similar transients in TREAT) or the pattern of cylindrical and radial cracks found in uranium oxide specimens given high-power, steady-state irradiations. All samples lost weight, which could not be accounted for by production of granular fragments (essentially no material of this nature was found). Even in the case of the highest-temperature exposure no pellets were found to be stuck to the cladding. Examination of the pellets and cladding showed no clear evidence for formation of interaction zones between fuel and tantalum.

Table IX. Inspection Summary

Sample	Maximum Recorded Cladding Temperature (°C)	Uranium Sulfide Weight Loss (%)	Comments
1	1060	1.7	Visual appearance identical with that of unexposed samples.
2	1265	1.7	Surface oxide layer gone from pellets. Some pellets fused together. Silvery gray matte surface on pellets.
3	1720	2.0	Appearance similar to that of Sample 2. Pellet diameters ranged about 0.003-0.01 cm larger than prior to exposure.
4	2000	2.0	Similar to Sample 3 except that some evidence was found that material from the pellets flowed against and was "cast" inside the cladding.
5	2390	3.0	Like Sample 4 except for extensive regions in which fuel was "cast" into the cladding.

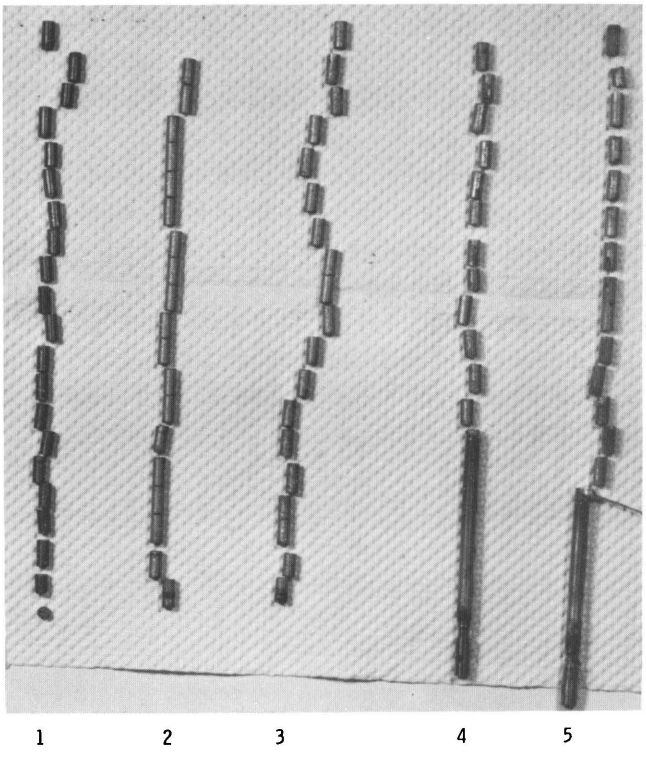

Figure 18

Appearance of US Fuel Pellets after Removal from Tantalum Jacket Tubes. Because of the increases in diameters of the pellets in Samples 4 and 5, the tantalum had to be peeled off in strips (however, the cladding did not adhere to the fuel in either case). The dark surface oxide film present on the sulfide prior to exposure is shown clearly for Sample 1, in contrast with the typical appearance of US after the higher-temperature exposures. Some evidence for flow of fuel material is apparent for Sample 5.

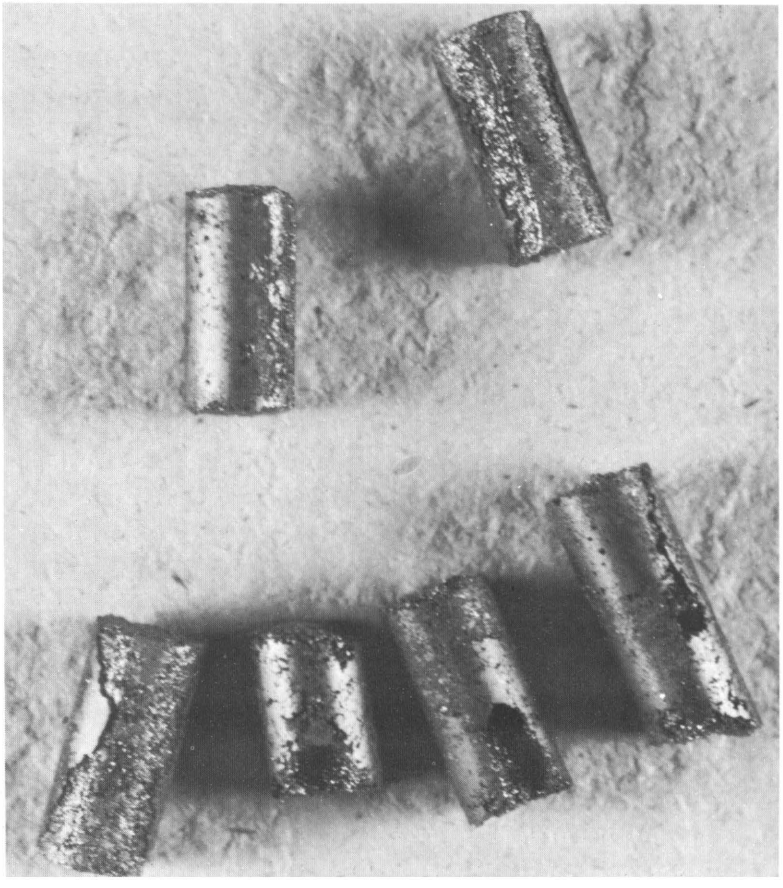

Figure 19

Close-up of Pellets from Sample 5, Showing More Clearly the Result of Flow and Solidification inside the Tantalum Tubing.

As originally loaded, the pellets had a thin (< 0.001 cm thick) oxide film resulting from grinding operations. Chemical analysis showed an insoluble residue, believed to be principally UOS, of about 4.75 w/o. This residue has been submitted for X-ray diffraction analysis. Samples from the five specimens have been set aside for chemical analysis, density measurements, and metallographic inspections.

Temperature data from the five samples were analyzed and compared against those from the tantalum-clad oxide samples run in the same meltdown equipment. With the aid of published values for the specific heats of tantalum and UO_2, an internally consistent relationship was obtained for the enthalpy of uranium sulfide, referred to room temperature, up to 1800°C. The average value of the specific heat over the range from 30°C to 1800°C was 0.037 cal/gm. A constant value of 0.046 cal/gm was found over the range from 1000°C to 1800°C. If it may be assumed that both uranium and sulfur each contribute their Dulong and Petit values to the specific heat, one can calculate a value of 0.0444 cal/gm at higher temperatures for the specific heat of uranium sulfide.

3. Pre-irradiated Fuel Elements

Suitable modifications were made to the remote encapsulation equipment for TREAT capsules to accommodate the loading of the pre-irradiated, short APDA fuel specimens. Four capsules were prepared containing one element each. These capsules were loaded into the shipping cask and are now ready for shipment to TREAT.

4. In-pile Oxidation Studies

Studies were continued on the determination of particle-size distribution that occurs when reactor fuels are heated in flowing air in a reactor environment.

A second pin of U-5% fissium, 20% enriched, was irradiated in flowing air in the TREAT reactor. The pin was supported in a BeO crucible on a tantalum-sheathed, W/W-26%Re thermocouple. Air was passed over the sample at a linear velocity of 8.5 ft/sec while the pin received an 81-Mw-sec transient. The maximum temperature recorded at the pin was 3220°C, and the first screen temperature rose 29°C (26° to 55°C).

The pin melted extensively and part of it dropped from its mount, hit the base of the thermocouple mount, and bounced into one of the louvered openings at the bottom of the crucible. This piece then burned or melted its way down through the 224-μ, 74-μ, and 25-μ screens. The sample continued down and hit the side of the 5-μ screen, cutting a vertical slit approximately $\frac{1}{8}$ in. wide and 5 in. long in this screen. Some bead formation occurred toward the bottom of the hole. One small piece hit the bottom area of the Millipore filter at the bottom of the capsule and discolored it locally without appreciable penetration.

The liquid nitrogen-cooled charcoal trap read 3 r/hr on the surface about 7-10 min after the shot.

During disassembly of the capsule, a small amount of material was lost. Analysis of the components of the capsule yielded these results:

BeO Crucible	689 mg
224-μ screen	18.4 mg
74-μ screen	17.3 mg
25-μ screen	133 mg
5-μ screen	319 mg
1-μ screen	56 mg
	~1233 mg or 1.233 g

The original pin weighed 1.3120 g, so that a loss of 79 mg, or 6%, occurred.

A new capsule has been designed and is now being built. This capsule will have upflow of air on the sample and then downflow on the screens, which should eliminate the falling down and rupturing of the screens by the pin. An attempt will be made to analyze a portion of the charcoal trap for uranium on the next run.

C. TREAT

1. Operation and Maintenance

Capsule 2B of the GE-APED Test Series on FCR fuel in TREAT was irradiated and returned to the Vallecitos Laboratory for examination.

CEN Metal-Water Reaction Test Series 29 was completed and the samples were returned to Argonne, Illinois, for examination. This series consisted of two experiments using 3-plate clusters of aluminum-clad, aluminum-uranium alloy fuel material in room-temperature water.

2. Large Sodium Loop

The large sodium loop which is being designed and constructed to provide a facility for the study of the meltdown of fuel clusters and subassemblies in TREAT is shown pictorially in Figure 20. The requirement for this loop originated as one of the facets of the fast reactor safety program. The loop will provide an environment of flowing sodium directed through the cluster of fuel pins while the reactor coincidentally supplies a transient pulse of thermal-neutron flux. The consequent generation of heat in the fuel will produce a rapid temperature rise in the coolant; with severe

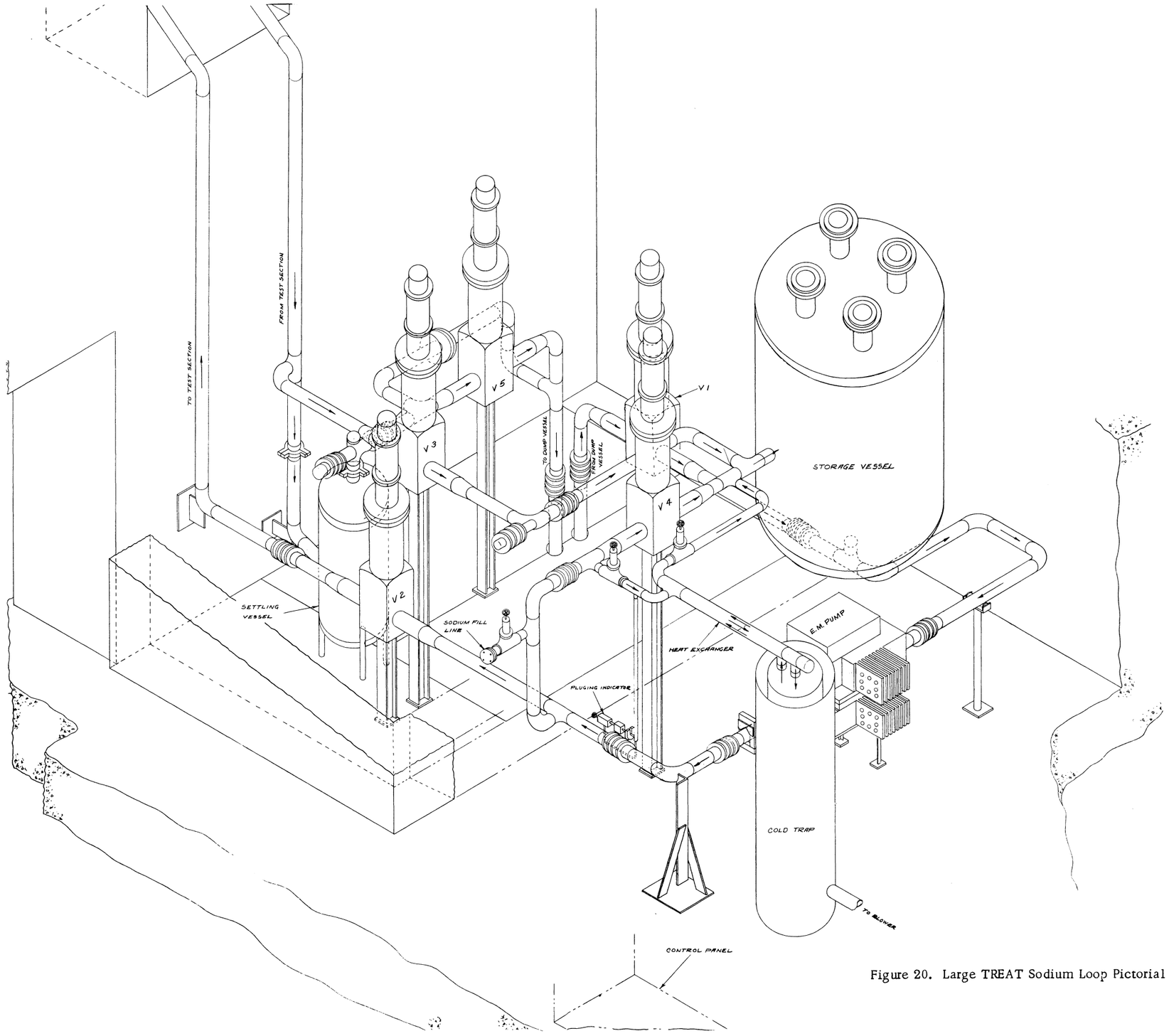

Figure 20. Large TREAT Sodium Loop Pictorial

enough transients and low sodium flows, boiling of the coolant and failure of the fuel will result. The studies carried out in this way will provide more realistic information on the manner in which the fuel may fail in a reactor core and the subsequent mechanisms of interaction in the system. In this way knowledge pertinent to future and present reactor designs will be obtained.

a. Description. The equipment for these experiments consists of an in-pile sodium-filled loop which is a semipermanent part of the reactor. The in-core section of the loop is a thimble housing the test specimen and is detachable from the remaining portion of the loop. This feature provides a means by which the reactor can be freed for other experiments when the loop is not in use. The flow design is shown in Figure 21.

The components of the loop as shown in Figure 21 are itemized. Located in the basement enclosure are:

1. an electromagnetic (EM) pump and associated rectifier;
2. five bellows-sealed P-K ball valves of 4-in. size, positioned in the loop circuit to provide control;
3. a cold trap in parallel with the main stream;
4. a plugging indicator cold trap which is used to monitor the oxide content of the loop.

A 3-in. stainless steel pipeline carries the sodium stream to the top of the reactor. The path of this line is upward through a cylindrical opening cast in the concrete in one side wall of the reactor. When the pipe exits from this cylindrical opening, it abruptly turns through 90° to pass horizontally above the top of the reactor core. Finally, this pipe terminates at the inlet side of the top of the test section. Three-inch Conoseal flanges are located at either end of the horizontal section of the pipe. These flanges are used for making a breakable connection to the test section and to permit removal of the horizontal pipe from above the core when access to the core is required.

A removable test section is positioned centrally and vertically in the reactor core (see Figure 22). This test section is so designed that the test specimen can be held vertically in the central region. The outer wall of the test section is of heavy-gauge stainless steel pipe. An annular channel formed between this pipe and a thin-gauge concentric inner shroud forms the downcoming channel. The incoming sodium enters this channel and travels downward to the bottom of the test section; at the bottom of the flow, direction is reversed 180° to enter the bottom of the test section chamber. The thin-gauge center tube located along the center axis of the test section houses the test specimen. The lower end of this center tube is not fastened to the outer structure but fits between concentric positioning guides.

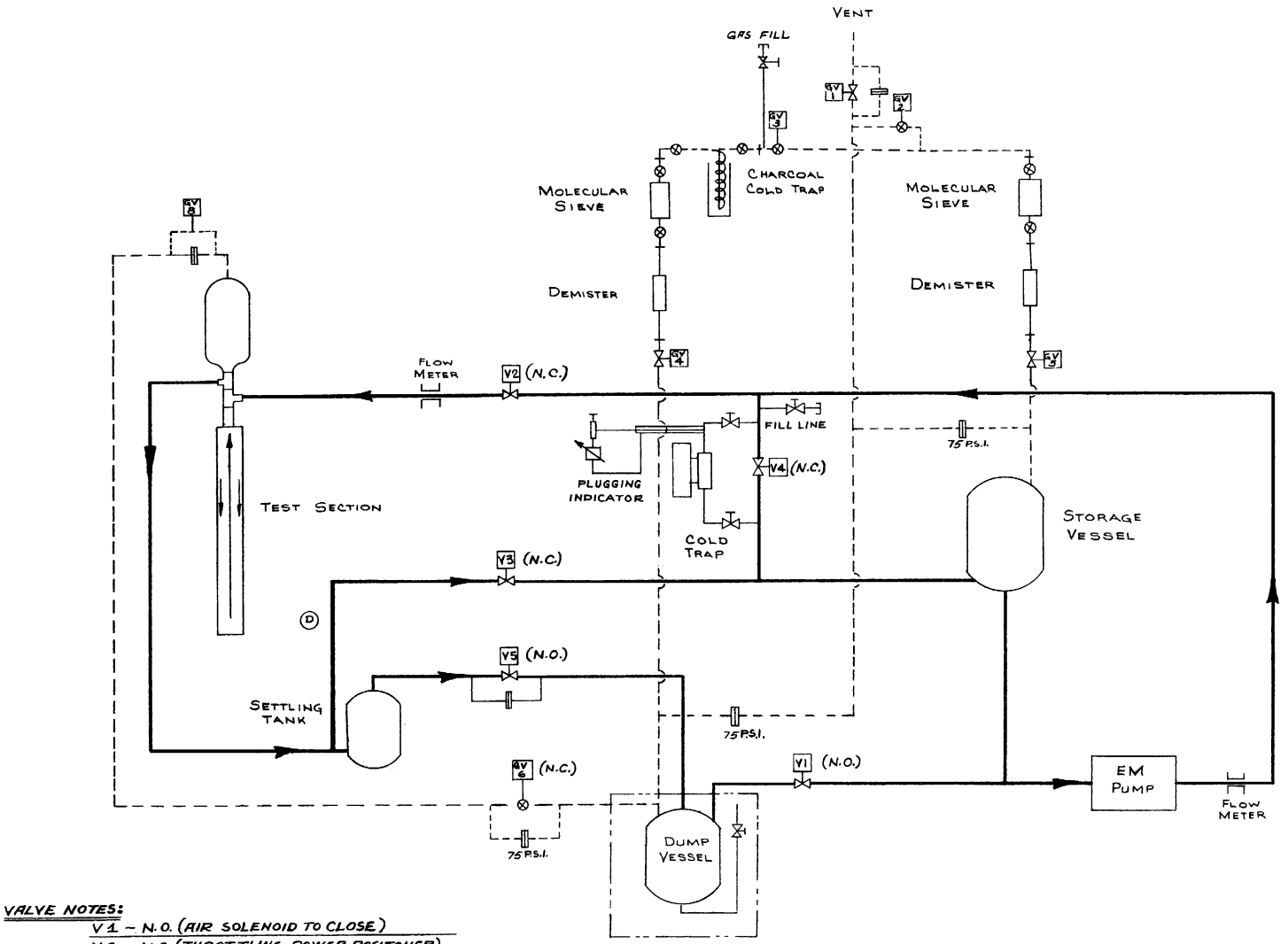

VALVE NOTES:

V 1 – N.O. (AIR SOLENOID TO CLOSE)
V 2 – N.C. (THROTTLING, POWER POSITONER)
V 3 – N.C. (AIR SOLENOID TO OPEN)
V 4 – N.C. (THROTTLING, POWER POSITONER)
V 5 – N.O. (AIR SOLENOID TO CLOSE)

Figure 21. Flow Diagram - Large TREAT Sodium Loop

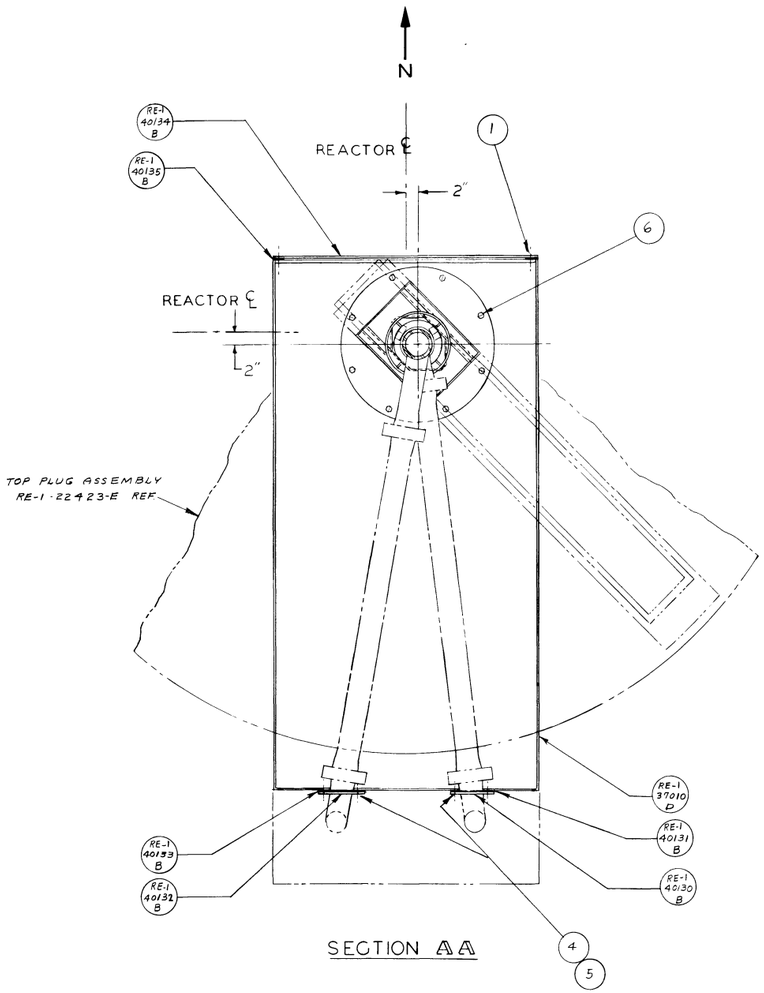

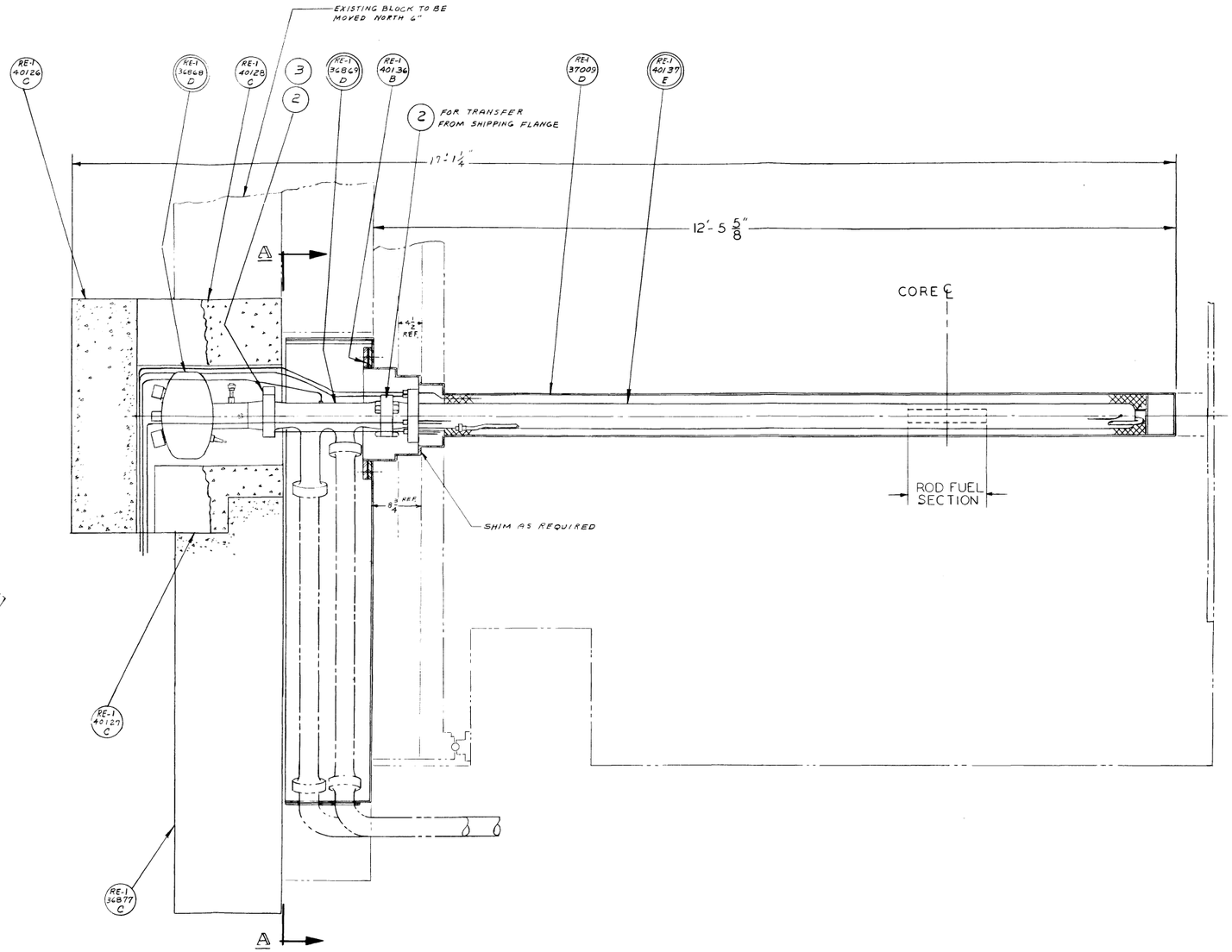

NOTES:
1. DESIGN DATA
   OPERATING PRESSURE - 75 PSI
   DESIGN PRESSURE - 150 PSI
   PSI OPERATING TEMP - 900°F
   PSI DESIGN TEMP. - 1025 °F
2. WELDING SPECIFICATIONS SEE RE-1-40141-B

Figure 22. Test Section. Large TREAT Loop.

At the upper end, this tube is clamped between the faces of the upper test-section flanges. A bellows spring loads an extension chamber which serves to lead the sodium from the specimen region to the outlet pipe of the test section. Sodium leaving the test section enters the downcomer pipe which leads the flow over the top of the reactor and down to the basement equipment room, where the sodium flows into the settling tank. This tank, a modified hydroclone of 24-gal capacity, serves as a trap for melted and subsequently solidified fuel particles. The sodium enters this chamber tangentially at the bottom; it follows a swirling path to the top of the tank, where it exits via a center opening. Upon leaving this tank the sodium can be directed in one of two directions by opening of proper valves. In one direction the sodium flows back to the storage vessel, thus completing the circuit of the loop. This mode of operation will be used when checkout of the system is made prior to excursion of an experimental transient. Otherwise, the sodium may flow into the dump vessel. This mode of operation will be used during a fuel meltdown. In this fashion, the contaminated sodium and fuel fragments will not be transferred to the storage tank, but will be led to the dump tank which is situated in a shielded floor enclosure.

During the transient meltdown, as the sodium is being transferred from the storage to the dump tank, an equal volume of gas must be led from the dump to the storage tank. This transfer is effected via the gas-transfer line shown in the schematic. Since some possibility exists that the gas may contain gaseous fission products and entrained sodium or vapor, the gas is led through a series train consisting of (1) a demister; (2) a molecular sieve column; and (3) a liquid nitrogen, charcoal cold trap. The cover gas chosen is helium. The gas-transfer line is also connected to the vent stack in the event that it is desired to dispose of the gas from either storage or dump vessel.

A valved (V-4) bypass line is connected from the upcoming line to the return side to the storage vessel. This line permits recirculating flow when the test section is isolated from this system or is not present. At this time, the in-pile section will be isolated by closing of valves V-2 and V-3. A second valved bypass line connected across V-4 is fitted with a cold trap and plugging indicator for the control and measurement of sodium purity.

The transfer of sodium will be made from the dump vessel to the storage vessel by pressurizing the dump vessel, closing valve V-5 and opening valve V-1. In this way the sodium will be raised from the lower elevation to the upper. Addition and removal of sodium will be performed by connecting a special portable sodium container to the valved fill line leading to the dump vessel.

b. Current Status of Loop. Calculations have been made pertinent to the performance features of the loop. In addition, the maximum expected

energy release associated with a total subassembly meltdown experiment has been estimated. The calculations are not ideal, since a scarcity of data and information exists to permit accurate estimates of interactions under such transient conditions. However, the estimates will be integrated into the hazards report which is currently being prepared.

At present, the design of the essential components of the loop has been practically completed. This includes such items as piping layout, tanks, test section, instrumentation circuitry, gas-transfer system, pump and rectifier arrangement, cold trap, plugging indicator, and shielding cask and handling system, which are now finished items. Still in the design stage are: (1) the electrical heater installation and (2) the sodium-transfer and loading equipment.

Equipment components now at the Idaho site consist of piping, instrumentation, recording equipment, and associated panels, shielding supports, electrical heater transformers, rectifier, electromagnetic pump, and piping expansion bellows. Some component tests have been carried out; results have indicated a need for repair and modification of the bellows and the air cylinders on the valves.

Thermal-shock and high-pressure exposure tests of the 3-in. Conoseal flange were satisfactorily performed. This test was performed in a sodium environment and served to demonstrate the adequacy of this type of connection.

The necessary building modifications have been completed. This consists of preparing the pit for the dump tank, repositioning the stairway leading to the subpile room, installation of transformers, design and installation of the equipment-handling crane, and purchase of the air-conditioning unit for cooling the basement.

Considering the present rate of progress, it is estimated that the loop will be ready about December, 1963.

VII. PUBLICATIONS

Papers

ALGORITHM 165, COMPLETE ELLIPTIC INTEGRALS
Henry C. Thacher, Jr.
Comm. Assoc. Computing Mach. 6, No. 4, pp. 163-164 (April, 1963)

CERTIFICATION OF ALGORITHM 55, COMPLETE ELLIPTIC INTEGRAL OF THE FIRST KIND and CERTIFICATION OF ALGORITHM 49, COMPLETE ELLIPTIC INTEGRAL
Henry C. Thacher, Jr.
Comm. Assoc. Computing Mach. 6, No. 4, pp. 166-167 (April, 1963)

CERTIFICATION OF ALGORITHM 147, PSIF
Henry C. Thacher, Jr.
Comm. Assoc. Computing Mach. 6, No. 4, p. 168 (April, 1963)

EQUIPMENT USED IN THE PERFORMANCE OF EXPERIMENTS IN NUCLEAR REACTORS AT THE ARGONNE NATIONAL LABORATORY
E. S. Sowa, C. R. Breden, and L. W. Fromm, Jr.
Nuclear Sci. and Eng. 15, pp. 415-428 (April, 1963)

NEUTRON ACTIVATION CROSS SECTION FOR Br^{79}, Br^{81}, Rh^{103}, In^{115}, AND I^{127}
S. A. Cox
Bull. American Physical Society 8, p. 335 (April, 1963)

P_3 DISTORTION FISSION OF U^{235} BY THERMAL 14-MeV NEUTRONS
A. M. Friedman, J. W. Meadows, P. R. Fields, and J. F. Whalen
Bull. American Physical Society 8, p. 369 (April, 1963)

FISSION CROSS SECTION OF Pu^{238}
D. K. Butler and R. K. Sjoblom
Bull. American Physical Society 8, p. 369 (April, 1963)

A STUDY OF CARRY-UNDER PHENOMENA IN VAPOR LIQUID SEPARATION
Michael Petrick
AIChE Journal 9 (2), 253-260 (March, 1963)

RF OSCILLATIONS AND POWER OUTPUT IN ALKALINE THERMIONIC CONVERTERS
H. K. Richards
Advanced Energy Conversion 2, 613-621 (1962)

DISCUSSION OF PAPER NO. 101

Raymond Viskanta

International Developments in Heat Transfer: Discussions. Am. Soc. Mech. Engrs., New York, 1963, p. D-267

DISCUSSION OF PAPER NO. 90

T. R. Bump

International Developments in Heat Transfer: Discussions. Am. Soc. Mech. Engrs., New York, 1963. pp. D-249 - D-250

DISCUSSION OF PAPER NO. 38

B. M. Hoglund

International Developments in Heat Transfer: Discussions. Am. Soc. Mech. Engrs., New York, 1963. p. D-125

AN AUTOMATIC RAPID SCANNING SPECTROPHOTOMETER TO STUDY THERMOLUMINESCENCE SPECTRA

A. K. Ghosh

Applied Optics 2 (3), 243-244 (March, 1963)

MANIPULATORS USED FOR HANDLING RADIOACTIVE MATERIALS

R. C. Goertz

Human Factors in Technology, ed. Edward Bennett, Jane Degan and Joseph Spiegel. McGraw-Hill, New York, 1963. Ch. 27, pp. 425-443

ELECTRONIC CONFIGURATION AND VALENCY OF URANIUM IN UCd_{11}, A MAGNETICALLY DILUTE ALLOY

F. A. Cafasso, H. M. Feder, and D. M. Gruen

J. Chem. Phys. 38 (5) 1256 (March 1, 1963). Letter

THE MECHANISM OF THE NICKEL-FLUORINE REACTION

R. L. Jarry, J. Fischer, and W. H. Gunther

J. Electrochem. Soc. 110 (4), 346 (April, 1963)

BURNING VELOCITIES OF URANIUM AND ZIRCONIUM IN AIR

L. Liebowitz, L. Baker, Jr., J. G. Schnizlein, L. W. Mishler, and J. D. Bingle

Nuclear Sci. and Eng. 15 (4), 395 (April, 1963)

THE EFFECT OF HALOGENATED HYDROCARBONS ON THE BURNING OF URANIUM AND ZIRCONIUM

L. Leibowitz, J. G. Schnizlein, and L. W. Mishler

Nuclear Sci. and Eng. 15 (4), 404 (April, 1963)

BURNING TEMPERATURES OF URANIUM AND ZIRCONIUM IN AIR

E. M. Mouradian and L. Baker, Jr.

Nuclear Sci. and Eng. 15 (4), 388 (April, 1963)

NEUTRON RADIOGRAPHY: 1962 PROGRESS REPORT
Harold Berger
Proceedings of the Symposium on Physics and Nondestructive Testing, pp. 175-197, Published by SW Res. Inst., San Antonio, Texas (1962)

ANL Reports

ANL-6411 SAFETY ANALYSIS REPORT, EBR-I, MARK IV
R. O. Haroldsen, F. D. McGinnis, M. Novick, L. R. Smith, and F. W. Thalgott

ANL-6625 LOCAL PARAMETERS IN COCURRENT MERCURY-NITROGEN FLOW
L. G. Neal

ANL-6630 LAMB WAVES: THEIR USE IN NONDESTRUCTIVE TESTING
Roberta Ann di Novi

ANL-6640 PROCEEDINGS OF THE AMU-ANL SUMMER STUDY PROGRAM, June 19-July 14, 1961
Amended Notes Edited by C. V. Pearson from Original Notes Compiled by G. E. Schweitzer

ANL-6664 TESTING OF CONTAINMENT CAPABILITIES OF REINFORCED CONCRETE-SHIELDED ENCLOSURES
S. H. Fistedis, A. H. Heineman, and M. J. Jancke

ANL-6667 A STUDY OF THE FLOW OF SATURATED FREON-11 THROUGH APERTURES AND SHORT TUBES
Hans K. Fauske and Tony C. Min

ANL-6690 CRITICAL STUDIES OF URANIUM-STEEL AND URANIUM-STEEL-SODIUM FAST REACTOR CORES (ZPR-III Assemblies 32 and 33)
P. I. Amundson, W. Gemmell, J. K. Long, and R. L. McVean